Bachelor's thesis

Direct Photon Production at the LHC

Submitted by

Lea Ziemons

August 30, 2023

First examiner
Priv.-Doz. Dr. Karol Kovařík

Second examiner
Dr. Tomáš Ježo

Universität Münster
Fachbereich Physik
Institut für Theoretische Physik

Contents

1. Abstract

In this thesis a first order prediction for the cross section of direct photon production in a proton proton collision is made and compared to experimental data from ALICE at an energy of $\sqrt{S}$=8 TeV.
The data is being met with an upward shift. The shape of the curve is predicted satisfactorily according to the limitations of the prediction. To improve the results higher orders and the masses of the quarks, which are set to zero here, need to be included. The dominant uncertainties are the scale error followed by the pdf error. The quark-gluon scattering is the most contributing process, followed by antiquark-gluon scattering for lower transversal photon momenta k_T and by quark-antiquark scattering for higher k_T, which shows the rapidly decreasing gluon pdf's for increasing Bjorken scale x. Up quarks contribute most to the cross section followed by charm quarks and then down quarks.

2. Introduction

What are we made of? What is the smallest existing particle? These are possibly the most famous questions. I remember learning about the raisin bun model in school, which is how people earlier thought atoms would look like. A positively charged dough with negatively charged raisins, randomly distributed. Nowadays they already teach that modelling the atom like a raisin bun is not appropriate and one rather looks at the atoms as a heavy nucleus and the electrons move around it in certain tracks.
The next question is: What is the nucleus made of (if it is not flour)? We learned that it is made of neutrons which are not electrically charged and protons which are positively charged. So, what are the protons and neutrons made of? I definitely heard the word quark in school, but to get a better understanding of the structure of protons I had to study physics. Then I learned that "what is something made of?" is not the only question to ask but "what keeps it together?" too. And here I am, in between I learned some more about physical theories but again asking the question, what are we made of? Now knowing that to understand the structure of protons I need to consider quantum theory or more accurate quantum field theory to get an idea about strong interaction and quarks. Thus, to what look? Particle physicist study the substructure of particles like atoms, their nuclei or hadrons like neutrons and protons by colliding them at very high energies and examining the decayed or even generated final state particles after the interaction.

Here I want to get an insight into the proton structure, accordingly I will look at a proton-proton collision. This collision can have many products. This thesis will focus on the production of photons, which are directly produced in the interaction of protons so called direct photons. The research question is: **How are direct photons created in a proton-proton collision? And what can be learned about the substructure of a proton from the cross section of direct photon production?**
Thus, the assumptions made for the strong interactions will be verified. Furthermore, it can be shown how photons can be produced directly from quarks and gluons as a consequence of the strong interaction.

To do so the thesis is structured as follows. First I will recap the theory (ch: 3) which is needed to calculate the cross section. The theory chapter is mainly based on literature by Halzen and Martin[8], Schwichtenberg [18] and Hollik [10]. It starts with the standard model and the basic interactions, then cross sections are introduced. After that, I will give a brief introduction about gauge theory to introduce Quantum Electro Dynamics and Quantum Chromo Dynamics which are the basis for the calculation. This leads to the feynman rules which are the practical rules to calculate the cross sections. Continuing with the strong coupling constant and finishing with parton distribution functions (pdf's). Then in the second part calculations are evaluated (ch: 4). First, the different processes and the corresponding feynman diagrams are discussed. Then for every process, the matrix elements are calculated. Following that we will have a closer look on the kinematics of the processes to get the cross section in its final form. In the next chapter (ch: 5) the theoretical calculation is compared to experimental data after finishing the numeric calculations. The thesis ends with a conclusion (ch: 6).

3. Theory

The goal of this thesis is to better understand the structure of protons by looking at collisions between them. Experiments reveal that protons have a substructure and are not the smallest entity. Fig: 1 shows schematically that protons consist of three valence quarks and in principal arbitrarily many sea quarks and gluons corresponding to the lowest plot. The sea quarks and gluons are created permanently by interaction between them. These are strong interactions.
How does strong interaction work? In this thesis, the production of photons is considered with proton-proton collision. The first learning is that not the protons are colliding but their constituents. In consequence it is a collision between quarks and gluons (see fig: 2). Thus, to have a look at the Standard Model first is useful.

3.1. Standard model

All particles can be fundamentally classified into two types: fermions and bosons. The difference is that fermions have a half-integer spin (the spin is a fundamental particle characteristic postulated in quantum mechanics). Matter consists primarily of fermions, the bosons however, are exchange particles and thus responsible for interaction and are integer-spin particles. This becomes clearer if one looks at the standard model with the fundamental particles (fig: 3).
It is structured in three blocks: quarks, leptons, and bosons. There are six quarks arranged in three generations. Each has $\frac{1}{2}$ spin (fermions) and $\frac{2}{3}$ (up, charm, and top quark) or $-\frac{1}{3}$ (donw, strange and bottom quark) electric charge. Then there are the leptons which are fermions as well (spin $\frac{1}{2}$), which are electron, myon, tauon and each has a corresponding neutrino. At last, there are the bosons, namely photons, W^+-,W^--and Z-boson, gluons and higgs boson.
These three blocks make more sense while considering the four fundamental interactions:

- electromagnetic interaction
- strong interaction
- weak interaction
- gravitation

Hence each interaction has its exchange boson or interaction boson which carries the charge. The electromagnetic interaction is mediated by photons, strong interaction by gluons, weak interactions by W^+,W^- and Z-bosons and for gravitation hints for the existence of an graviton are searched for.
Quarks interact strongly, weakly and electromagneticly. The leptons are divided in

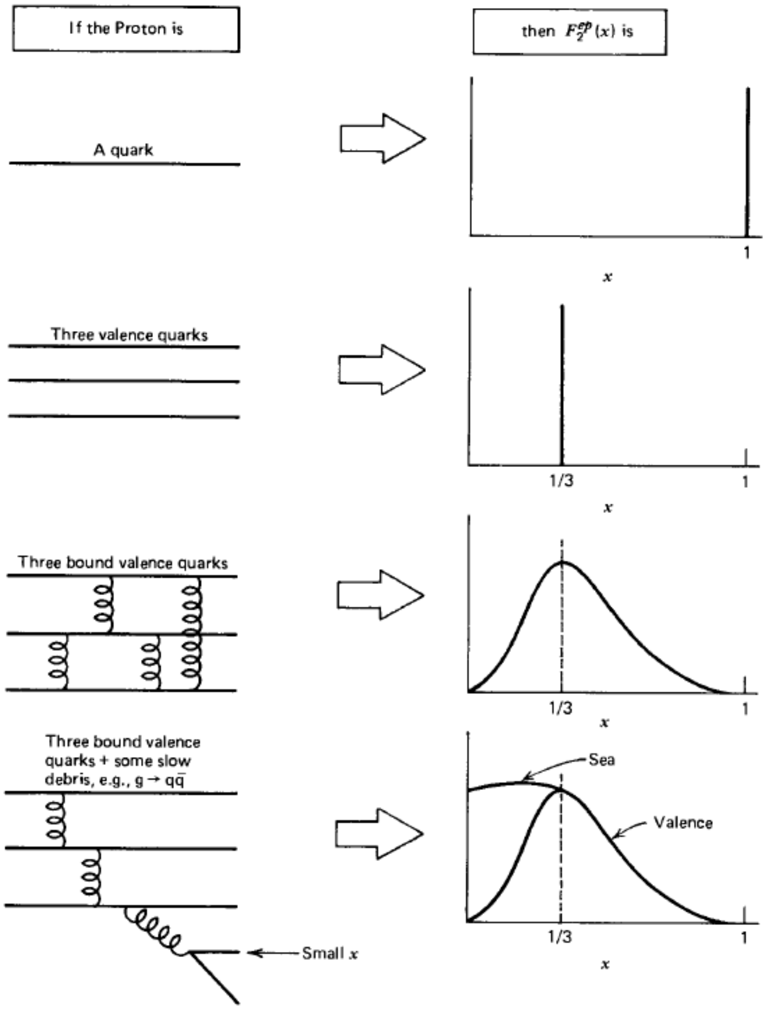

Figure 1: Shown is a schematic illustration of the possible components of a proton and the effect on the structure function $F(x)$ [8].

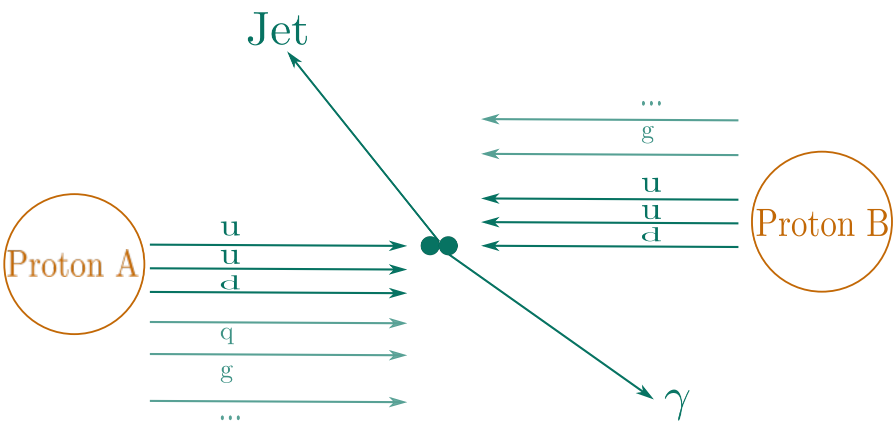

Figure 2: The sketch of the proton proton collision illustrates the underlying parton collision. The blurred arrows correspond to the sea quarks.

electron, muon, and tauon. They interact electromagnetic and weak and the neutrinos

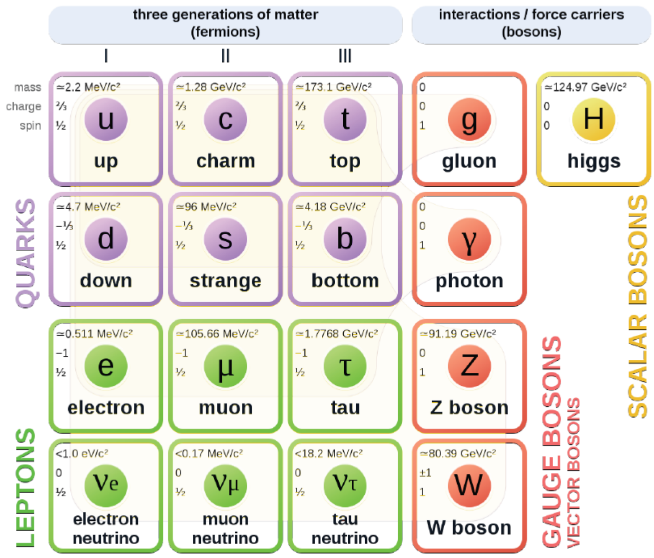

Figure 3: Shown is the standardmodel of particle physics [3].

only weak.
Every particle from the standard model has a corresponding antiparticle, which is the same in every characteristic but the charges have negative signs.
So for the consideration of the proton collisions the quarks of which the protons consist are relevant. Furthermore the strong interaction and with it the gluons. Since direct photon production is considered, also the electromagnetic interaction must be looked at.
Here is a table (tab: 1) which shows the masses of the different quarks which are relevant for the calculation:

quark	mass M
up	2.16 MeV
down	4.67 MeV
strange	93.4 MeV
charm	1.27 GeV
bottom	4.18 GeV
top	around 170 GeV

Table 1: The tab shows the masses of the different quarks in natural units [19].

3.1.1. Colors and strong interaction

This thesis is about proton collision. Speaking about interactions, we can now more accurately say, their components are interacting strongly and electromagnetically. What does a proton look like?

$$p = uud \tag{1}$$

That means that a proton consists of two up quarks and one down quark, these are the three valence quarks. There are more sea quarks and gluons which appear through strong interaction. The quarks are produced in quark antiquark pairs: $u\bar{u}, d\bar{d}, c\bar{c}, s\bar{s}, t\bar{t}, b\bar{b}$.
Looking at the valence quarks there is an illustrative way to see the necessity of introducing color. The proton has an anti symmetric ground state due to uud. But the

Δ^{++}-baryon has three up-quarks ($\Delta^{++} = uuu$). This is equivalent to a completely symmetric wave function which breaks the Pauli principle. To solve this, color or differently said a new charge can be introduced, also answering the question of why single quarks are never observed. There are three colors red, blue, and green, and their three anticolors. All particles which can be observed are white, which means they either have all three colors or anticolors, or are color anticolor pairs. See for example proton, antiproton, and pion in fig: 4.

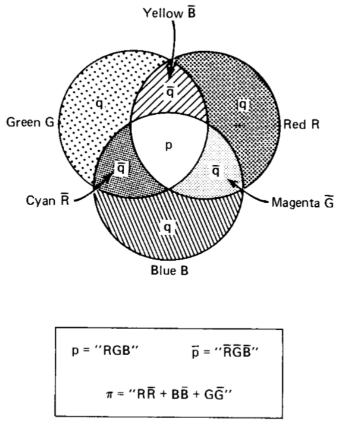

Figure 4: The figure shows the color composition of proton, antiproton and pion [8].

Strong interaction then is the exchange of color between quarks and gluons. In contrast to electromagnetic interaction, where the photon is uncharged the gluons are charged, gluons have color, more accurate they always carry a color and an anticolor and therefore can interact as well. Hence, gluons can interact with themselves.

3.2. Cross section

Now coming back to the proton proton collision where quarks and gluons interact. So what are we looking at now? The cross section is the central value of all the calcuations. What is the cross section? [1]
There is a number of particles scattered at a scattering center in a certain unit of time, which is called $\frac{N}{\Delta t}$. This number of particles is proportional to the Luminosity L which is the number of particles in a time unit per transverse area unit at the scattering center. The proportionality factor is the cross section σ. So the cross section is kind of the probability of a scattering event.
Normally one is not interested in the total cross section, but in the differential cross section, in other words, the cross section in a certain angular range $d\Omega$. Mathematically said:

$$\frac{dN}{d\Omega} = \frac{d\sigma}{d\Omega}\, L. \tag{2}$$

The cross section is so useful because the luminosity L is a collision characteristic, so if the cross section is calculated, one knows how many particles N in which angular range $d\Omega$ scatter.
In quantum mechanics the differential cross section can be written as[16]:

$$d\sigma = \frac{1}{F}\, M^2\, d\mathrm{PS}_n. \tag{3}$$

[1]The answer given in the following is based on [9].

Here, F is the flux factor, M the matrix element and $d\text{PS}_n$ the phase space integral which is Lorentz invariant.

3.3. Gauge theory

To get the cross section one needs to calculate the matrix element for which quantum field theory is needed. The matrix element M is the probability of a particle in an initial state $\langle in|$ going to an outgoing state $|out\rangle$:

$$|M|^2 \sim \langle \text{in}| \ldots |\text{out}\rangle \,. \tag{4}$$

In this chapter the whole quantum field theory cannot be explained or derived, nevertheless a brief motivation is given: What is the basic idea and how are the feynman rules derived from this, which are the basis of the calculation of the matrix element in the second part?
Even though Gauge theory is mathematically complicated and looks kind of unnatural sometimes it has one big advantage: it can describe all the mechanics (classical, electromagnetic and quantum mechanics).
So what is the fundamental idea? All particle actions underlay local gauge symmetries. These symmetries are connected to conservation laws by the Lagrangian formalism.
The Lagrange formalism is known from classical mechanics: There is an action S, which is Lorentz-invariant:

$$S = \int dt \; L. \tag{5}$$

This action has to be minimised which leads to the Lagrange's Equations which are fundamental equations of motion:

$$\frac{d}{dt}\left(\frac{\partial L}{\partial \dot{q}_i}\right) - \frac{\partial L}{\partial q_i} = 0. \tag{6}$$

q_i are the generalised coordinates of the particles, t the time, here L has to be chosen right and is $L = T - V$, which is the difference between kinetic energy T and the potential energy V. Extending this formalism to fields, one gets the Euler-Lagrange equation:

$$\frac{d}{dx_\mu}\left(\frac{\partial \mathscr{L}}{\partial(\partial\phi/\partial x_\mu)}\right) - \frac{\partial \mathscr{L}}{\partial \phi} = 0. \tag{7}$$

$\mathscr{L}$ is the Lagrange density, just called Lagrangian from now on. Then the action looks like follows:

$$S = \int d^4x \; \mathscr{L}. \tag{8}$$

This S follows certain rules, is for example invariant for Lorentz transformations and has symmetries. Therefore, knowing S allows to get information about the field. The task then is to choose the Lagrangian's for the different problems.

3.3.1. Quantum electro dynamics (QED)

To get from classical to quantum mechanics the fields also have to be quantized, which is done by a quantized wave function ψ and the fields are operators now. Starting with

Quantum Electro Dynamics means to looking at electromagnetic interaction only. One sets the condition of local invariance. In this case of QED it is an U(1) transforamtion:

$$\psi(x) \rightarrow e^{i\alpha(x)}\psi(x). \tag{9}$$

This invariance leads to the Lagrangian:

$$\mathscr{L}_{QED} = -\frac{1}{4}F_{\mu\nu}F^{\mu\nu} + e\bar{\psi}\gamma_\mu\psi A^\mu + \bar{\psi}(i\gamma^\mu\partial_\mu - m)\psi. \tag{10}$$

F are the electromagnetic field tensor from electrodynamics and A the electromagnetic fields. e is the electric charge and ψ the wave functions. The γ-matrices are the dirac matrices. The first summand corresponds to the electromagnetic waves, the second to the interaction and the last to mechanical electrons.

3.3.2. Quantum chromo dynamics (QCD)

Now how to get from QED to Quantum Chromo Dynamics? One extends the condition for phase invariance of an U(1) group to a SU(3) group:

$$\psi_i \rightarrow U_{ij}\psi_j = e^{i\alpha^a T^a_{ij}}\psi. \tag{11}$$

U is part of the SU(3) group, which consists of unitary 3×3 matrices. T^a_{ij} is the base of Lie algebra, the generator of the group and consists of a=8 3×3 matrices. a corresponds to the eight different gluons due to the 8 combinations of three colors and anticolors. T thus follows the Lie algebra with the structure constant f_{abc}:

$$[T_a, T_b] = if_{abc}T_c. \tag{12}$$

This becomes important for the interaction between gluons (first summand of equation: 13), which however is not relevant for the process discussed here. In order to keep the Lagrangian invariant under this phase transformation it must be adjusted as follows:

$$\mathscr{L}_{QCD} = -\frac{1}{4}G^a_{\mu\nu}G^{\mu\nu\ a} + \bar{\psi}_i(i\gamma^\mu\not{\partial} - m_q)\delta_{ij}\psi_j - g_s\bar{\psi}_i\gamma^\mu T^a_{ij}\psi_j G^a_\mu. \tag{13}$$

The wave functions ψ are fields with i,j=1,2,3 each component has four-components again. The slashed partial derivation is a short form to wright $\not{\partial} = \partial_\mu\gamma^\mu$. As well gauge fields G^a_μ were introduced and the strong interaction constant g_s, which will be discussed further in chapter 3.5. Here, the first term corresponds to gluon gluon interaction, the second to free quarks and the last to gluon quark interaction.

3.3.3. From the Lagrangian to matrix element

How to get from the Lagrangian's to the matrix element M needed for the cross section?[2] In quantum mechanics the Hamilton principle is used, where a time evolution operator $\hat{U}(t, t_0) = e^{-\frac{i}{\hbar}\hat{H}(t-t_0)}$ describes the development of time of a state. Looking for a transition amplitude from one state to another one generalised to $G(x'', t; x', t_0) = \langle x''| \hat{U}(t, t_0) |x'\rangle$. Then a wave function can be written as another wave function with a corresponding transition amplitude G:

$$\psi(x'', t) = \int d^3x'\ G(x'', t; x', t_0)\ \psi(x', t_0). \tag{14}$$

[2] This subsection bases on [15].

Now G is the connection to the Lagrangian approach because G can be written as:

$$G(x_f, t_f, x_i, t_i) = \int \mathscr{D}[x(t)] e^{\frac{i}{\hbar} S[x(t)]}, \tag{15}$$

where $\hat{S}$ is the operator to the action S (eq: 8) the integral over the Lagragian density $\mathscr{L}$ and $\mathscr{D}$ is the integral over all possible paths for fixed endpoints x_i and x_f. Because S is related to the Lagrangian $\mathscr{L}$ (eq: 8) then the Lagrangian's from QED (eq: 10) and QCD (eq: 13) can be filled in to get the matrix element:

$$|M|^2 \sim \langle in| \, G \, |out\rangle \, . \tag{16}$$

To solve this equation a perturbation theory approach is used where, in simple terms, the first relevant order of the exponential function series is considered. Thus, the feynman rules can be derived, which goes beyond the scope of this bachelor thesis.

3.4. Feynman rules

The Feynman rules are an outcome of the gauge theory and an illustrative way to calulate the matrix elements for the cross section. They are external lines (corresponding to the interacting particles) and internal lines (which correspond to the propagator) and vertices (the interactions).
Starting with the **external lines** which in our case can be quarks (17), antiquarks (18), photons (19) and gluons(20):

Ingoing quark: 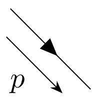

$= u(p)$ Outgoing quark: 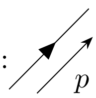

$= \bar{u}(p)$ (17)

Ingoing antiquark: 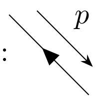

$= \bar{v}(p)$ Outgoing antiquark: 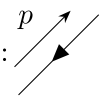

$= v(p)$ (18)

Ingoing photon: 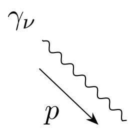

$= \epsilon_\nu(p)$ Outgoing photon: 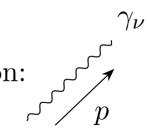

$= \epsilon^*_\nu(p)$ (19)

Ingoing gluon: 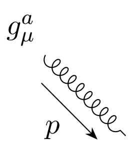

$= \epsilon^a_\mu(p)$ Outgoing gluon: 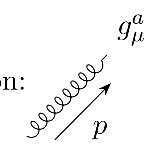

$= \epsilon^a_\mu(p)$ (20)

Here u,v are spinors (describing the spins) and ϵ_μ or ϵ_ν describe the transversal polarisation. They depend on the corresponding momentum p of the particle.
The **internal lines**, in the case here, quarks and antiquarks (21), with the masses of the quarks m and there momenta p:

quark: 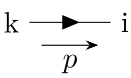

$= \delta^{ki} \dfrac{i(\not{p} + m)}{p^2 - m^2}$ antiquark: 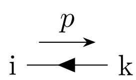

$= \delta^{ik} \dfrac{i(\not{p} + m)}{p^2 - m^2}$ (21)

Lastly, looking at the **vertices**. First with two quarks and a gluon and then with two antiquarks and a gluon (22), two quarks and a photon and two antiquarks and a photon (23):

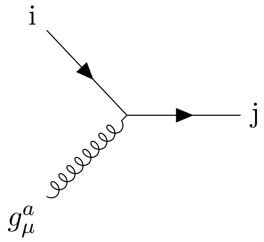

$$= i\ g_s\ T^a_{ji}\ \gamma^\mu$$

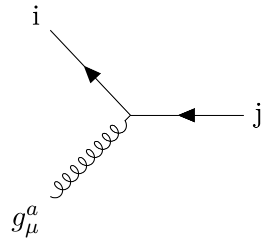

$$= i\ g_s\ T^a_{ij}\ \gamma^\mu \tag{22}$$

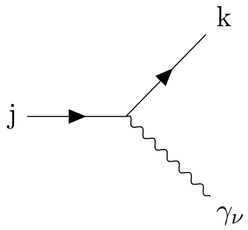

$$= i\ e_f\ e\ \gamma^\nu$$

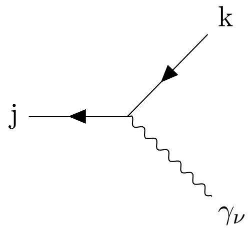

$$= i\ e_f\ e\ \gamma^\nu \tag{23}$$

Here the strong coupling constant g_s (further discussed in ch: 3.5), the coupling of the electromagnetic interaction $e \cdot e_f$ which is the charge of the quark, T^a which are the generators of the color group SU(3) and the γ-matrices need for the solution of the Dirac-equations, are introduced.
After identifying the feynman diagrams for the process, these feynman rules are used to calculate the matrix elements M.

3.5. Strong coupling constant

The coupling constant α_s (connected to g_s through eq: 97) must be considered in more detail in QCD because it is not a constant but depends on the scale Q^2 with an arbitrary size.[3] This is due to the fact that a perturbation-theoretical approach was chosen. If all orders would be included there would be no dependency on Q but if only one order or two orders are included the strong coupling constant depends on Q.
The relation of α_s and Q is given by:

$$\alpha_s(Q^2) = \frac{4\pi}{\beta_0 \ln\left(\frac{Q^2}{\Lambda^2}\right)} \tag{24}$$

with

$$\Lambda^2 = \mu^2\ e^{-\frac{4\pi}{\beta_0}\alpha_s(\mu^2)} \tag{25}$$

and

$$\beta_0 = 11 - \frac{2}{3}n_f. \tag{26}$$

n_f is number of different quark flavors, μ^2 is the scale used at which $\alpha_s(\mu^2)$ is a constant. Two things should be emphasised: First there is an asymptotic freedom, because the coupling decreases, which means that for large Q the particles act like free particles,

[3]As a literature basis for this chapter [5] and [10] are used.

which makes it legitimate to use perturbative theory for the strong interaction. Second for small Q the coupling constant α_s diverges so the coupling gets really strong.
The strong coupling constant then can be measured in experiments. Normally, the scale of the Z-boson is choosen, so that[19]

$$\mu = m_z = 91.19\,\text{GeV}, \text{and } \alpha_s(\mu^2) = 0.1179. \tag{27}$$

The coupling constant plotted over the scale Q is shown in Fig. 5.

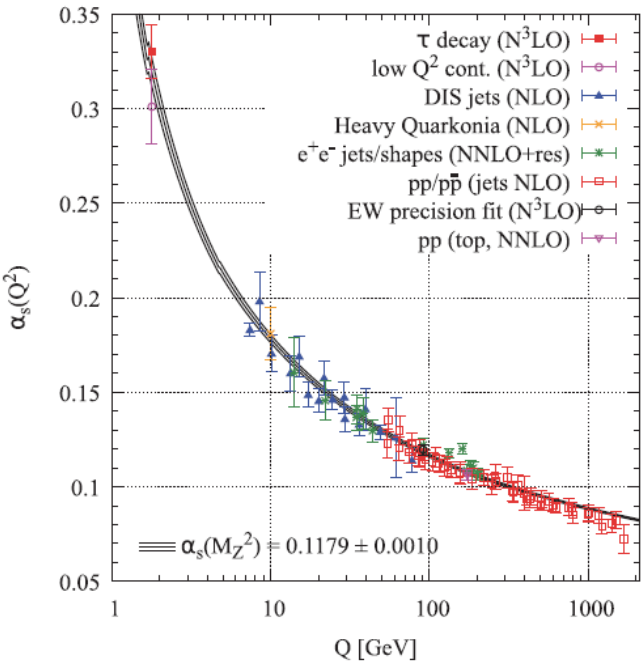

Figure 5: It is shown the theoretical prediction of the strong coupling constant α_s in first order with the experimental data at different scales Q [10].

3.6. Parton distribution functions (pdf's)

It is now known how the cross section for the collision of two quarks or gluons can be calculated. But in the experiment not two protons but quarks and gluons collide, these are called partons, since there are parts of the proton. So how does one know which particles of the respective protons will collide? One cannot know, but the parton model suggests that protons consist of partons. All of these partons possess a fraction of the proton energy and momentum. This fraction is called Bjorken variable x which indicates which four momenta share a parton has of the total particle.
The parton distribution functions $P(x)$ are the probability density of a parton, which describe the probability of finding a parton with a momentum fraction x within the proton. Per definition the sum over all partons i integrated over x is one:

$$\sum_i \int dx\; xP_i(x) = 1. \tag{28}$$

Since a proton proton collision at high energies is considered, its partons act as nearly free particles.
The pdf's are the means to conclude from the cross section on parton level to the cross

section on proton level. In fig: 6 the pdf's for different quarks and gluons can be seen for two scales $Q = 10$ GeV and $Q = 70$ GeV corresponding to the momentum range looked at in the comparison to experimental data later. $x \cdot P(Q, x)$ is shown with their pdf uncertainty ΔP_{pdf} calculated with (in analogy to the pdf uncertainty discussed in ch: 5.6.2)[14]:

$$\Delta x P_{pdf} = \frac{1}{2}\sqrt{\sum_k (xP(f_k^+) - xP(f_k^-))^2}. \tag{29}$$

The pdf set CT18NNLO[11] is used because it is the latest of the CT sets and NNLO is next to next to leading order which is the most accurate including two orders. First of

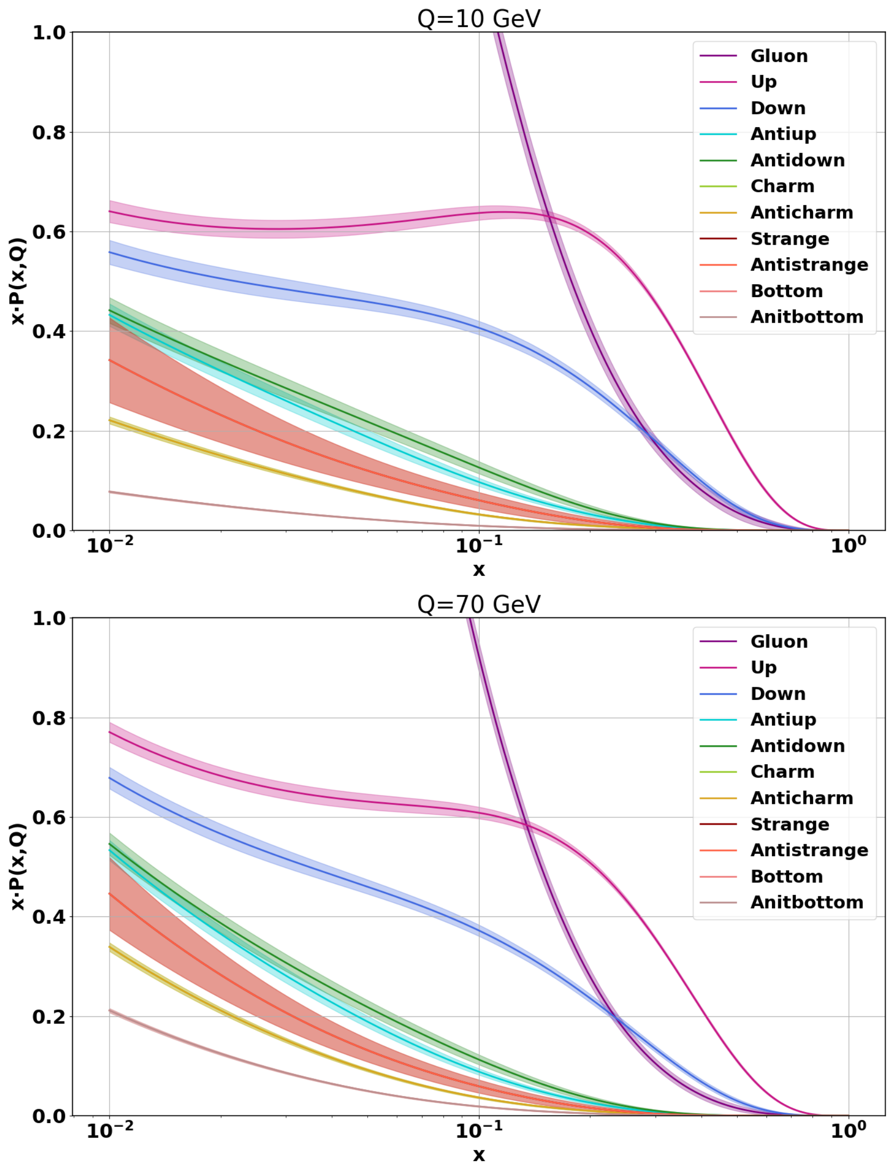

Figure 6: Shown are the pdf's at $Q = 10.0$ GeV and $Q = 70.0$ GeV for the different partons. Pdf $P(Q, x)$ times bjorken variable x over x. $x \cdot P(Q, x)$ is shown with the corresponding pdf uncertainties $\Delta\sigma_{pdf}$.

all, it is recognisable that for x going to one $x \cdot P(x, Q)$ for all partons goes to zero, which matches with the expectation that a proton does not consist of just one particle which would be the case if one particle would have had the total momentum. Furthermore, for little momentum fractions the gluon is dominant and then decreasing rapidly for increasing x. Also the diagrams show the peaks of the valence up and down quarks and that the peak of the down quark is about half of the up quark. The probability of finding a quark increases with decreasing x for all quark flavors. Note however, that some flavors are more suppressed due to its much higher mass. In addition for a lower scale Q the peak of the valence quarks is bigger and the probability of sea quarks lower. In the following figure (fig: 7) only the pdf's for antiparticles is shown to get a closer look needed in the discussion later. To get the cross section one has to integrate over all

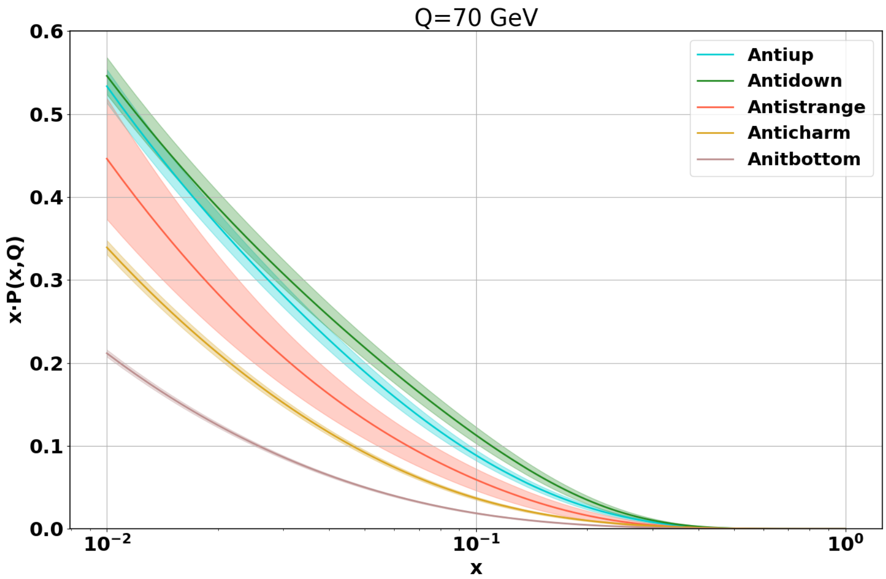

Figure 7: Pdf's only anti particles by Q=70.0 GeV for antiquarks only. Pdf P(Q,x) times bjorken variable x over x.

the energy fractions for each parton and multiply with the pdf's[9]:

$$\sigma(AB \to FX) = \sum_{a,b} \int dx_1 \int dx_2 \, P_{a/A}(x_1, Q^2) \, P_{b/B}(x_2, Q^2) \, \hat{\sigma}(ab \to F). \tag{30}$$

A and B denote the two protons, F is the final state, here a direct photon and X the rest, which is a quark, an antiquark or a gluon (see in ch: 4.1). These particles hadronize and will be seen in the experiment as jets. a and b then are the partons colliding and $P_{a/A}(x_1, Q^2), P_{b/B}(x_2, Q^2)$ their corresponding pdf's. $\hat{\sigma}(ab \to F)$ is the cross section at parton level.
The actual pdf's are numerical calculations, trying functions to fit with the measured data.

3.7. Direct photon production

An idea how to calculate the cross section was evaluated after it was demonstrated that when protons collide their components, the quarks and gluons, interact with each other. What are direct photons? One calls a produced photon a direct photon if they originate in the interaction of gluons and quarks. Contrary photons that arise in the parton shower or due to Bremsstrahlung are not direct photons. So in the case of direct photons the

quark interacts electromagneticly while the strong interaction of a gluon and an (anti-)quark happens simultaneously. This is possible because quarks have a color and an electric charge.
In this case one can see the different Lagrangians ($\mathscr{L}_{QED}$ and $\mathscr{L}_{QCD}$) as a sum so the first interaction comes from the $\mathscr{L}_{QCD}$, this gets clearer when the feynman diagrams are drawn in chapter 4.1.

4. Theoretical prediction

The calculation splits in two main parts. First, the matrix elements for the different parton proccesses need to be calculated (ch: 4.1) . Then, to get from the parton cross sections to a measurable cross section kinematics need to be considered (ch: 4.2).

4.1. Matrix elements

Starting with the matrix elements M: Reminding the feynman rules from ch: 3.4. Several additional rules regulate which processes are allowed, i.e. which combinations of our incoming and outgoing particles, propagtors and vertices are valid and produce direct photons:
1. The fermion line must be continuous and consistent in direction.
2. Vertices can consist of two quarks and one gluon, or two quarks and a photon. (Deriving from the feynman rules also vertices with three gluons exist, but they do not matter looking at direct photon production because there are no vertices consisting of gluons and photons (gluons have no electromagnetic charge).
3. Electric and color charge has to be conserved in a vertex.
Also here only first order diagrams are considered, meaning no loops are allowed.

In consequence direct photons can be produced in three possible processes in proton-proton collisions. These are shown below in the form of feynman diagrams. The first process is **quark-gluon scattering**, where the s- (fig: 9a) and u-channels (fig: 9b) are possible. One process is determined by the same input and output particles. The different channels mean that different interaction (vertices) can lead to the same output. The naming convention is inspired by the mandelstamm variables (see app:106) because the squared momentum of the propagator is equivalent to the corresponding mandelstamm variable. The second process is the same only that an antiquark is scattering with a gluon (**antiquark-gluon scattering**), there is also the s-channel (fig: 10a) and the u-channel (fig: 10b). The last process is **quark-antiquark scattering** you can see the t-channel (fig: 11a) and the u-channel (fig: 11b) below. In the following for each of the three processes the matrix elements which are directly connected to the cross sections (eq: 3) are calculated.

They are more processes leading to the same result but including loops means higher orders. These are not considered for the prediction as here only a first order prediction is made. Here (fig: 8) is just one example given of how a higher order diagram would look like:

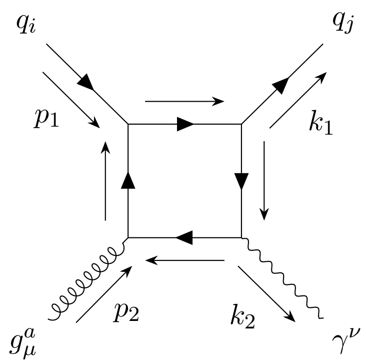

Figure 8: Here an example of a second order feynman diagram for quark-gluon scattering is illustrated.

4.1.1. Quark-gluon scattering

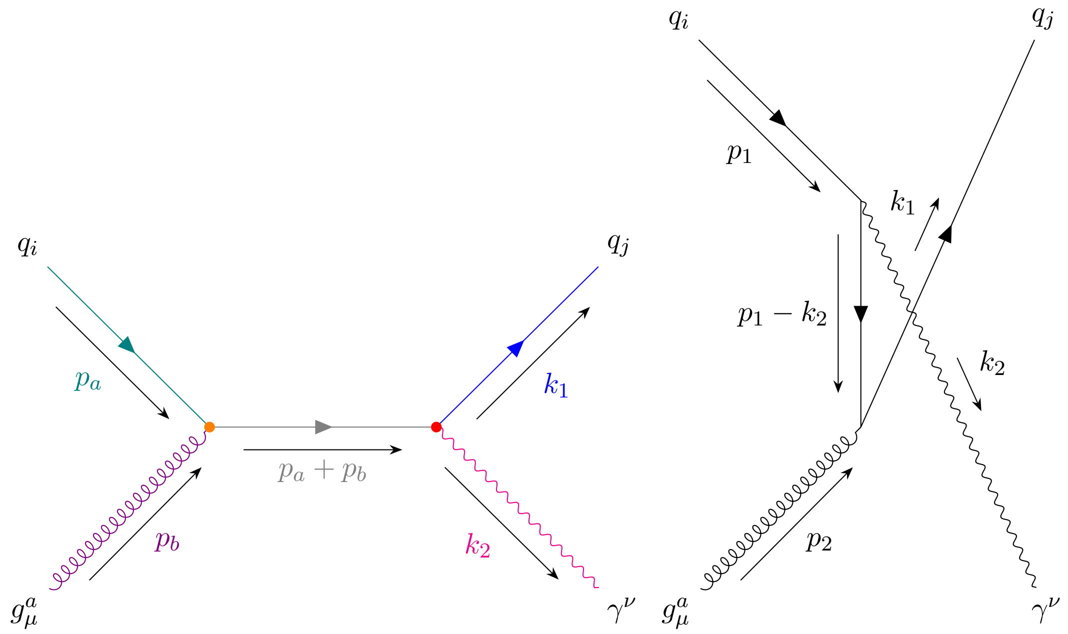

Figure 9: The figure shows the two (u- and s-channel) feynman diagramms for quark-gluon scattering. Also there is a color coding to illustrate eq: 32

The feynman rules (derived in ch:3.4) are used to calculate the matrix elements. Starting with the first process quark-gluon scattering in fig: 9. The full matrix element M_1 is the sum of the s- (M_{1s}) (fig: 9a) and u-channel (M_{1u}) (fig: 9a), also the interference term has to be added, which can be simplified as shown below:

$$\begin{aligned} M_1^2 &= M_{1s}^2 + M_{1u}^2 + M_{1s}^\dagger M_{1u} + M_{1s} M_{1u}^\dagger \\ &= M_{1s}^2 + M_{1u}^2 + 2\ \mathrm{Re}(M_{1s} M_{1u}^\dagger) \end{aligned} \tag{31}$$

Starting with M_{1s} combining the different terms of the feynman rules (eq: 17-23) together and using momentum conversion ($\mathbf{p} = \mathbf{p_a} + \mathbf{p_b}$). The bold momenta symbolize four-vectors. For the first matrix element M_{1s} the feynman diagram (fig: 9a) is shown and the different parts colored as the corresponding terms in the equation.

$$\begin{aligned} M_{1s} = &-\frac{i \cdot e \cdot e_f \cdot g_s}{\mathbf{p}^2 - m_q^2} \bar{\varepsilon_\mu}(\mathbf{p_b}) \bar{\varepsilon}^*_\nu(\mathbf{k_2}) \cdot \delta_{kj}\ T^a_{ij} \\ &\bar{u}^{s_1}(\mathbf{k_1}) \bar{\gamma}^\nu((\mathbf{p_a} + \mathbf{p_b})^\alpha\ \bar{\gamma}^\alpha + m_q)\bar{\gamma}^\mu u^{s_2}(\mathbf{p_a}). \end{aligned} \tag{32}$$

Then the adjoint is:

$$\begin{aligned} M^\dagger_{1s} = &\frac{i \cdot e \cdot e_f \cdot g_s}{\mathbf{p}^2 - m_q^2} \bar{\varepsilon'_\mu}^*(\mathbf{p_b}) \bar{\varepsilon}_{\nu'}(\mathbf{k_2}) \cdot \delta_{kj}\ T^a_{ij} \\ &\bar{u}^{s_2}(\mathbf{p_a}) \bar{\gamma}^{\mu'}((\mathbf{p_a} + \mathbf{p_b})^{\alpha'}\ \bar{\gamma}^{\alpha'} + m_q)\bar{\gamma}^{\nu'} u^{s_1}(\mathbf{k_1}). \end{aligned} \tag{33}$$

Here e_f is the share of e from the charge of the quark (see tab: 3). The color part can be considered seperately which leads to:

$$\begin{aligned} M_{1s,Color} &= \delta_{ij} T^a_{jk} \\ M^\dagger_{1s,Color} &= \delta_{ij} T^a_{kj} \\ \Rightarrow M^2_{1s,Color} &= T^a_{ki} T^a_{ik} = Tr(T^a T^a) = \frac{1}{2}\delta^{aa}. \end{aligned} \tag{34}$$

Averaging over the colors of the quark ($\frac{1}{N}$) and the gluon ($\frac{1}{N^2-1}$) and sum the eight ($N^2 - 1$) color combinations, $\overline{M_{1,s,color}}^2$ yield:

$$\overline{M_{1,s,color}}^2 = \frac{1}{N} \frac{1}{N^2 - 1} \sum_a^{N^2-1} \frac{1}{2} \delta^{aa} = \frac{1}{2N}. \tag{35}$$

It has to be averaged over the colors of quark and gluon because there is no way to know the color of the quark and the gluon.
Now the rest of M^2_{1s} needs to be transformed before in the end adding the color factor again:

$$\begin{aligned} M'^2_{1s} = &\frac{(e\ e_f\ g_s)^2}{(\mathbf{p}^2 - m_q^2)^2} \bar{\varepsilon_\mu}^*(\mathbf{p_b}) \bar{\varepsilon}_\nu(\mathbf{k_2}) \bar{\varepsilon'_\mu}^*(\mathbf{p_b}) \bar{\varepsilon}_{\nu'}(\mathbf{k_2}) \\ &\bar{u}^{s_1}(\mathbf{k_1}) \bar{\gamma}^\nu\ (\mathbf{p_a} + \mathbf{p_b})^\alpha\ \bar{\gamma}^\alpha + m_q)\bar{\gamma}^\mu u^{s_2}(\mathbf{p_a}) \\ &\bar{u}^{s_2}(\mathbf{p_a}) \bar{\gamma}^{\mu'}\ (\mathbf{p_a} + \mathbf{p_b})^{\alpha'}\ \bar{\gamma}^{\alpha'} + m_q)\bar{\gamma}^{\nu'} u^{s_1}(\mathbf{k_1}). \end{aligned} \tag{36}$$

First one can sum over the polarisation using $\sum \bar{\varepsilon_\mu}(p_b)\bar{\varepsilon}^*_{\mu'}(p_b) = g_{\mu\mu'}$ and $\sum \bar{\varepsilon_{\nu'}}(k_2)\bar{\varepsilon}^*_\nu(k_2) = g_{\nu'\nu}$ which results in:

$$\begin{aligned} M'^2_{1s} = &\frac{(e\ e_f\ g_s)^2}{(\mathbf{p}^2 - m_q^2)^2} \bar{u}^{s_1}(\mathbf{k_1}) \bar{\gamma}_\nu\ ((\mathbf{p_a} + \mathbf{p_b})^\alpha\ \bar{\gamma}^\alpha + m_q)\bar{\gamma}^\mu u^{s_2}(\mathbf{p_a}) \\ &\bar{u}^{s_2}(\mathbf{p_a}) \bar{\gamma}_\mu\ ((\mathbf{p_a} + \mathbf{p_b})^{\alpha'}\ \bar{\gamma}^{\alpha'} + m_q)\bar{\gamma}^\nu u^{s_1}(\mathbf{k_1}). \end{aligned} \tag{37}$$

Then one sums over the spins s_1, s_2 using the completeness relation
$\sum_{s_i} u^{s_i}(p)\bar{u}^{s_i}(p) = \not{p} + m$ and also identify a trace:

$$M'^2_{1s} = \frac{(e\ e_f\ g_s)^2}{(\mathbf{p}^2 - m_q^2)^2} \mathrm{Tr}((\not{\mathbf{k}}_1 + m_q)\gamma_\nu(\mathbf{p}_\alpha\gamma^\alpha + m_q)\gamma^\mu(\not{\mathbf{p}}_a + m_q)\gamma_\mu(\mathbf{p}'_{\alpha'}\gamma^{\alpha'} + m_q)\gamma^\nu). \tag{38}$$

At this point the quark masses are set to zero ($m_q \approx 0$), because they are small (see 1) compared to the considered centre of mass energy of $\sqrt{S}$=8 TeV. The validity of the approximation is is discussed in ch: 5.4. So neglecting the masses it follows:

$$M_{1s}'^2 = \frac{(e\ e_f\ g_s)^2}{\mathbf{p}^4} \mathbf{k_{1}}_{,\beta}\ \mathbf{p}_\alpha\ \mathbf{p_{a}}_{,\delta}\ \mathbf{p}_{\alpha'}\ \mathrm{Tr}(\gamma^\beta \gamma_\nu \gamma^\alpha \gamma^\mu \gamma^\delta \gamma_\mu \gamma^{\alpha'} \gamma^\nu). \tag{39}$$

Using γ-matrix identities (see 103, 104) the trace can be solved and also $\mathbf{p} = \mathbf{p_a} + \mathbf{p_b}$ is used which leads to:

$$M_{1s}'^2 = 16 \left(\frac{e\ e_f\ g_s}{s}\right)^2 [(\mathbf{k_1} \cdot \mathbf{p})(\mathbf{p} \cdot \mathbf{p_a}) - (\mathbf{k_1} \cdot \mathbf{p_a})(\mathbf{p} \cdot \mathbf{p}) + (\mathbf{k_1} \cdot \mathbf{p})(\mathbf{p_a} \cdot \mathbf{p})]. \tag{40}$$

Before continuing it is useful to have a closer look at the scalar products which can be reformulated using the mandelstamm variables (A.2.1) one can write:

$$\begin{aligned} s = (\mathbf{p_a} + \mathbf{p_b})^2 &= \mathbf{p_a^2} + \mathbf{p_b^2} + 2\mathbf{p_a} \cdot \mathbf{p_b} \\ \Rightarrow \mathbf{p_a} \cdot \mathbf{p_b} &= \mathbf{k_1} \cdot \mathbf{k_2} = \frac{1}{2} s \qquad (41) \\ \mathbf{p_a} \cdot \mathbf{k_2} &= \mathbf{p_b} \cdot \mathbf{k_1} = -\frac{1}{2} u \qquad (42) \\ \mathbf{p_a} \cdot \mathbf{k_1} &= \mathbf{p_b} \cdot \mathbf{k_2} = -\frac{1}{2} t. \qquad (43) \end{aligned}$$

Then follows for M_{1s}^2:

$$M_{1s}'^2 = -8(e\ e_f\ g_s)^2 \frac{u}{s}. \tag{44}$$

Now the color factor (eq: 35) is added again and the spins from the initial particles (quark and gluon) are averaged (because here analogue to the colors, the spin of the initial particles is unknown) which gives a factor of $\frac{1}{2}$ for each:

$$\overline{M_{1s}}^2 = -\frac{1}{N}(e\ e_f\ g_s)^2 \frac{u}{s}. \tag{45}$$

Analogously the matrix element M_{1u} for the u-channel (fig: 11b) can now be calculated. Using the feynman rules there is the following ansatz:

$$\begin{aligned} M_{1u} = &- \frac{i \cdot e \cdot e_f \cdot g_s}{\mathbf{p}^2 - m_q^2} \bar{\varepsilon_\mu}(\mathbf{p_b}) \bar{\varepsilon}_\nu^*(\mathbf{k_2}) \cdot \delta_{jk}\ T^a_{kj} \\ &\bar{u}^{s_1}(\mathbf{k_1}) \bar{\gamma}^\nu\ ((\mathbf{p_a} - \mathbf{k_2})^\alpha\ \bar{\gamma}^\alpha + m_q) \bar{\gamma}^\mu u^{s_2}(\mathbf{p_a}) \qquad (46) \\ M_{1u}^\dagger = &\frac{i \cdot e \cdot e_f \cdot g_s}{\mathbf{p}^2 - m_q^2} \bar{\varepsilon}_\mu'^{\,*}(\mathbf{p_b}) \bar{\varepsilon}_{\nu'}(\mathbf{k_2}) \cdot \delta_{jk}\ T^a_{kj} \\ &\bar{u}^{s_2}(\mathbf{p_a}) \bar{\gamma}^{\mu'}\ ((\mathbf{p_a} - \mathbf{k_2})^{\alpha'}\ \bar{\gamma}^{\alpha'} + m_q) \bar{\gamma}^{\nu'} u^{s_1}(\mathbf{k_1}). \qquad (47) \end{aligned}$$

The color factor is completly analogous:

$$\overline{M_{1,u,color}}^2 = \frac{1}{2N}. \tag{48}$$

The rest of the calculation is also analogous only that **p**=**p$_\mathbf{a}$**-**k$_\mathbf{2}$**. One gets:

$$\overline{M_{1u}}^2 = -\frac{1}{N}(e\ e_f\ g_s)^2 \frac{s}{u}. \tag{49}$$

Now the interference term is calculated:

$$
\begin{aligned}
M_{1s}M_{1u}\dagger =& \frac{(e\ e_f\ g_s)^2}{(\mathbf{p}^2-m_q^2)(\mathbf{p'}^2-m_q^2)}\bar{\varepsilon_\mu}(\mathbf{p_b})\bar{\varepsilon}^*_\nu(\mathbf{k_2})\bar{\varepsilon'_\mu}^*(\mathbf{p_b})\bar{\varepsilon}_{\nu'}(\mathbf{k_2}) \\
& \bar{u}^{s_1}(\mathbf{k_1})\bar{\gamma}^\nu\left(\mathbf{p}^\alpha\bar{\gamma}^\alpha+m_q\right)\bar{\gamma}^\mu u^{s_2}(\mathbf{p_a}) \\
& \bar{u}^{s_2}(\mathbf{p_a})\bar{\gamma}^{\mu'}\left(\mathbf{p'}^{\alpha'}\bar{\gamma}^{\alpha'}+m_q\right)\bar{\gamma}^{\nu'}u^{s_1}(\mathbf{k_1})
\end{aligned} \tag{50}
$$

where $\mathbf{p}$ and $\mathbf{p'}$ are $\mathbf{p}$=$\mathbf{p_a}$+$\mathbf{p_b}$ and $\mathbf{p'}$=$\mathbf{p_a}$-$\mathbf{k_2}$. Setting the quark mass to zero results in:

$$
M_{1s}M_{1u}\dagger = \frac{(e\cdot e_f\cdot g_s)^2}{(\mathbf{p}^2\cdot\mathbf{p'}^2)}p_\alpha\ p_{\alpha'}\ k_1^\beta\ p_a^\delta\ Tr(\gamma^\beta\gamma_{\nu'}\gamma^\alpha\gamma^\mu\gamma^\delta\gamma_{\nu'}\gamma^{\alpha'}\gamma_\mu). \tag{51}
$$

Using γ-identities (app: 103, app 104) the equation evolves to:

$$
M_{1s}M_{1u}\dagger = -32\frac{(e\ e_f\ g_s)^2}{us}(\mathbf{p}\cdot\mathbf{p'})(\mathbf{k_1}\cdot\mathbf{p_a}). \tag{52}
$$

Which simplifies to:

$$
M_{1s}M_{1u}\dagger = \frac{(e\ e_f\ g_s)^2}{N}\frac{t(s+t+u)}{us}. \tag{53}
$$

Using the relation that $s+u+t$ is proportional to the masses squared (app: 107) in the case that masses are set zero the interaction term is zero. Now we can write the total cross section for the quark-gluon-process, which is with eq: 31 in the case of $m_q=0$:

$$
\overline{M_1^2} = -\frac{(e\ e_f\ g_s)^2}{N}\left(\frac{u}{s}+\frac{s}{u}+\cancel{2\frac{t(s+t+u)}{us}}\right). \tag{54}
$$

It is also possible to not approximate the masses as zero. Therefore, the calculation is made by mathematica[12]. Accordingly mathematica calculates anagolous to the hand calculation and keeps the masses. This results in the following matrix element[12]:

$$
\begin{aligned}
\overline{M_1^2} =& \frac{(e\ e_f\ g_s)^2}{N\left(m_q^2-s\right)^2\left(m_q^2-u\right)^2} \\
& (16m_q^8-4m_q^6(s+u)+m_q^4\left(9s^2-52su+9u^2\right) \\
& +m_q^2\left(s^3+13s^2u+13su^2+u^3\right)-su\left(s^2+u^2\right)).
\end{aligned} \tag{55}
$$

4.1.2. Antiquark-gluon scattering

Let's go to the second process in fig: 10. This case is almost analogous to the quark-gluon scattering. Looking at the M_s (fig: 10a) and M_u (fig: 10b) the difference is only the v instead of the u spinors (the color factor is already omitted here):

$$
\begin{aligned}
M'_{2s} =& -\frac{i\cdot e\cdot e_f\cdot g_s}{\mathbf{p}^2-m_q^2}\bar{\varepsilon_\mu}(\mathbf{p_b})\bar{\varepsilon}^*_\nu(\mathbf{k_2})\cdot\delta_{kj}\ T^a_{ij} \\
& \bar{v}^{s_1}(\mathbf{k_1})\bar{\gamma}^\nu\left((\mathbf{p_a}+\mathbf{p_b})^\alpha\bar{\gamma}^\alpha+m_q\right)\bar{\gamma}^\mu v^{s_2}(\mathbf{p_a})
\end{aligned} \tag{56}
$$

$$
\begin{aligned}
M'_{2u} =& -\frac{i\cdot e\cdot e_f\cdot g_s}{\mathbf{p}^2-m_q^2}\bar{\varepsilon_\mu}(\mathbf{p_b})\bar{\varepsilon}^*_\nu(\mathbf{k_2})\cdot\delta_{jk}\ T^a_{kj} \\
& \bar{v}^{s_1}(\mathbf{k_1})\bar{\gamma}^\nu\left((\mathbf{p_a}-\mathbf{k_2})^\alpha\bar{\gamma}^\alpha+m_q\right)\bar{\gamma}^\mu v^{s_2}(\mathbf{p_a}).
\end{aligned} \tag{57}
$$

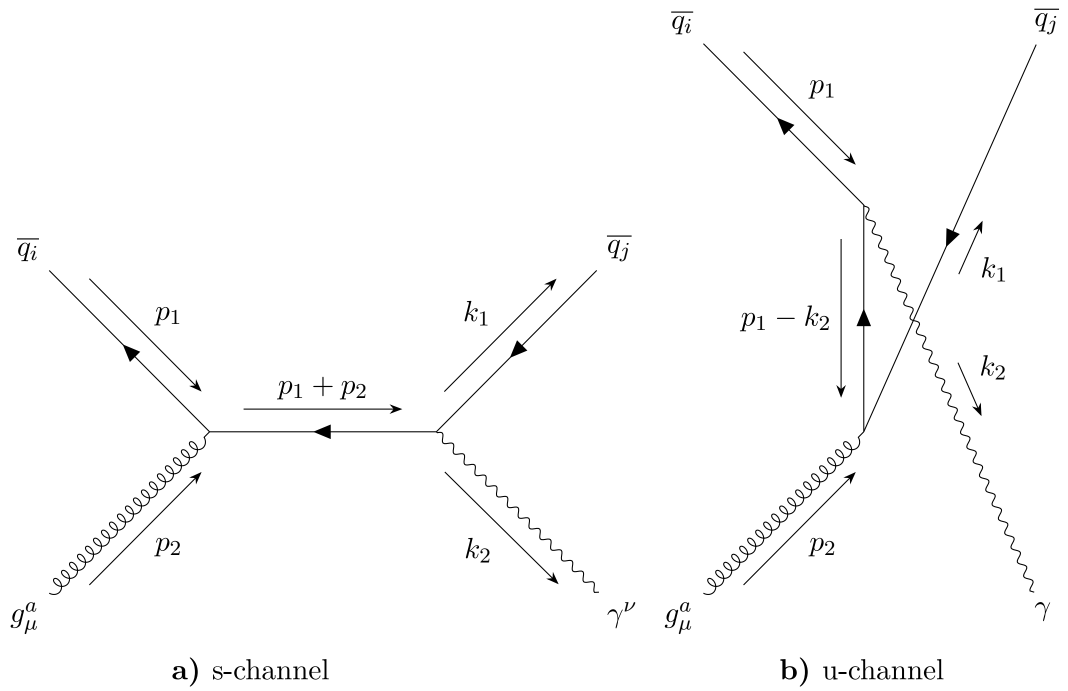

Figure 10: The figure shows the feynman two (s- and u-channel) diagrams for antiquark-gluon scattering.

Now considering that the sum of the u-spinors is $\sum_{s_i} u^{s_i}(p)\bar{u}^{s_i}(p) = \not{p} + m$ and $\sum_{s_i} v^{s_i}(p)\bar{v}^{s_i}(p) = \not{p} - m$ there is a sign switch in the mass terms. So in the case of $m_q = 0$ the result is the same and even considering the masses one will see that there only exist even exponents of the mass terms ($\overline{M^2} \propto m^{2n}$) so that the antiquark-gluon scattering and quark-gluon scattering has the same results:

$$\overline{M_2^2} = \overline{M_1^2}. \tag{58}$$

4.1.3. Antiquark-quark scattering

Now the process in fig: 11 has to be analysed, an antiquark and quark scatter to a photon and gluon. Starting with the t-channel (11a) the cross section without the color-term with $\mathbf{p} = \mathbf{p_b} - \mathbf{k_2}$, is:

$$\begin{aligned} M'^2_{3t} =& \frac{(e\ e_f\ g_s)^2}{(\mathbf{p}^2 - m_q^2)^2} \bar{v}^{s_1}(\mathbf{p_b})\bar{\gamma}_\nu(\mathbf{p}^\alpha\bar{\gamma}^\alpha + m_q)\bar{\gamma}^\mu u^{s_2}(\mathbf{p_a}) \\ & \bar{u}^{s_2}(\mathbf{p_a})\bar{\gamma}_\mu(\mathbf{p}^{\alpha'}\bar{\gamma}^{\alpha'} + m_q)\bar{\gamma}^\nu v^{s_1}(\mathbf{p_b}). \end{aligned} \tag{59}$$

This leads to:

$$\overline{M_{3t}^2} = \frac{N^2-1}{N^2}(e\ e_{f2}\ g)^2\ \frac{u}{t}. \tag{60}$$

Looking at the u-channel (fig: 11b), $\mathbf{p} = \mathbf{p_a} - \mathbf{k_2}$:

$$\begin{aligned} M'^2_{3u} =& \frac{(e\ e_f\ g_s)^2}{(\mathbf{p}^2 - m_q^2)^2} \bar{v}^{s_1}(\mathbf{p_b})\bar{\gamma}^\mu(\mathbf{p}^\alpha\bar{\gamma}^\alpha + m_q)\bar{\gamma}^\nu u^{s_2}(\mathbf{p_a}) \\ & \bar{u}^{s_2}(\mathbf{p_a})\bar{\gamma}^{\nu'}(\mathbf{p}^{\alpha'}\bar{\gamma}^{\alpha'} + m_q)\bar{\gamma}^{\mu'} v^{s_1}(\mathbf{p_b}) \end{aligned} \tag{61}$$

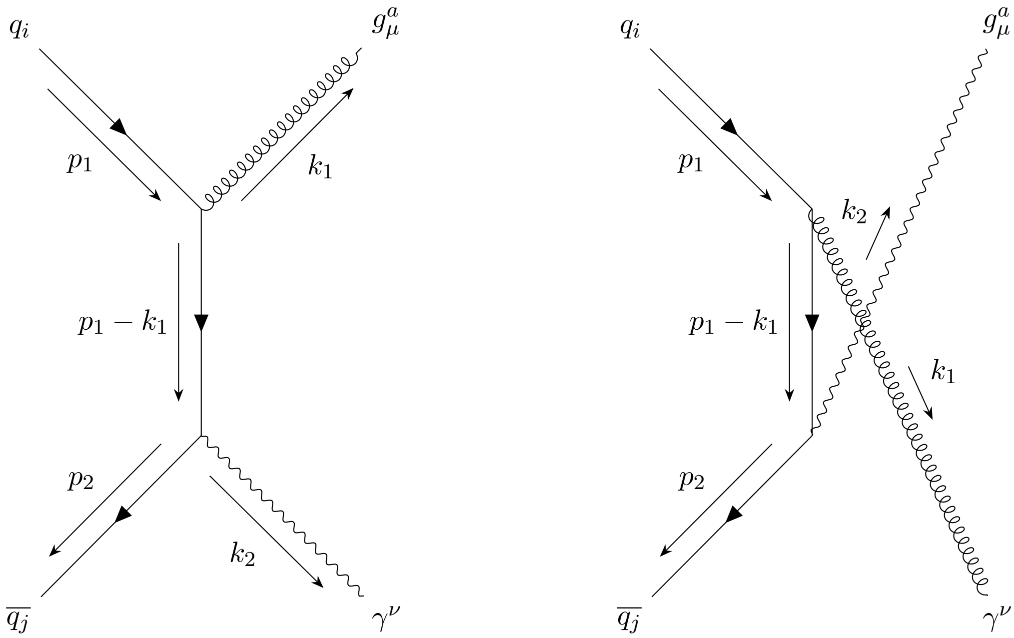

a) t-channel **b)** u-channel

Figure 11: The figure shows the two (t- and s-channel) feynman diagramms for antiquark-quark scattering.

which is:

$$\overline{M_{3u}^2} = \frac{N^2-1}{N^2}(e\ e_f\ g_s)^2\ \frac{t}{u}. \tag{62}$$

The interference term with $\mathbf{p} = \mathbf{p_b} - \mathbf{k_2}$ and $\mathbf{p'} = \mathbf{p_a} - \mathbf{k_2}$ is:

$$\begin{aligned} M'_{3u}M'_{3t}\dagger = & \frac{(e\ e_f\ g_s)^2}{(\mathbf{p^2} - m_q^2)(\mathbf{p'^2} - m_q^2)} \bar{v}^{s_1}(\mathbf{p_b})\bar{\gamma}^\nu(\mathbf{p}^\alpha\bar{\gamma}^\alpha + m_q)\bar{\gamma}^\mu u^{s_2}(\mathbf{p_a}) \\ & \bar{u}^{s_2}(\mathbf{p_a})\bar{\gamma}^{\nu'}(\mathbf{p}^{\alpha'}\bar{\gamma}^{\alpha'} + m_q)\bar{\gamma}^{\mu'} v^{s_1}(\mathbf{p_b}). \end{aligned} \tag{63}$$

Finally the result is:

$$\overline{M_{3t}M_{3u^\dagger}} = -\frac{N^2-1}{N^2}(e\ e_f\ g_s)^2\ 2s(s+t+u). \tag{64}$$

Then the matrix element for the antiquark-quark scattering looks like:

$$\overline{M_3^2} = \frac{N^2-1}{N^2}(e\ e_f\ g_s)^2\ \left(\frac{t}{u} + \frac{u}{t} - \cancel{2s(s+t+u)}\right). \tag{65}$$

Here one can also include the masses in Mathematica and gets[12]:

$$\begin{aligned} \overline{M_3}^2 = & -\frac{(e\ e_f\ g_s)^2\left(N^2-1\right)}{N^2\left(m_q^2-t\right)^2\left(m_q^2-u\right)^2} \\ & (6m_q^8 + 9m_q^6(t+u) + 2m_q^4\left(t^2 - 30tu + u^2\right) \qquad (66) \\ & + m_q^2\left(t^3 + 16t^2u + 16tu^2 + u^3\right) - tu\left(t^2+u^2\right)). \qquad (67) \end{aligned}$$

All needed matrix elements are summarised in tab: 2 and also compared to the results from [7].

4.2. Kinematics

Thus, the matrix elements are calculated and the cross section can be easily calculated for the partonic process using eq: 3. At the experiment one "sees" only the protons collide. Accordingly one has to do some kinematics and have closer look at the collision to get the cross section for the proton proton collision. The sketch (fig: 12) shows schematically the

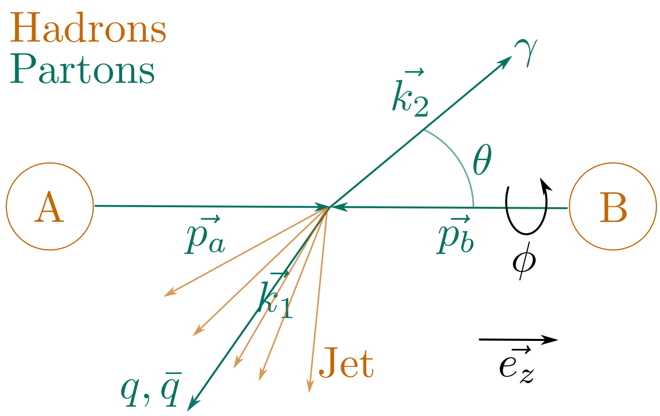

Figure 12: This is a sketch of the proton proton collision.

collision process. There are two input particles and two output particles. This process is first calculated at the parton level. So there is:

$$\begin{aligned}
\text{Parton in 1}: \vec{p_a}\,(\text{momenta}), E_a\,(\text{energy}) \\
\text{Parton in 2}: \vec{p_b}\,(\text{momenta}), E_b\,(\text{energy}) \\
\text{Parton out 1}: \vec{k_1}\,(\text{momenta}), E_1\,(\text{energy}) \\
\text{Parton out 2}: \vec{k_2}\,(\text{momenta}), E_2\,(\text{energy}).
\end{aligned}$$

First of all it is useful to keep in mind that one has to distinguish between two systems. Calculating the cross sections the partons (quarks and gluons) were looked at. The partons live in the first system let's call it the "small center of mass" system from now on SCMS. In this SCMS the whole energy can be expressed as $E_{SCMS} = E_a + E_b$ the same for the momentum $\mathbf{p} = \mathbf{p_a} + \mathbf{p_b}$, in addition it applies:

$$\begin{aligned}
\mathbf{p_a} = \mathbf{k_1} = -\mathbf{p_b} = -\mathbf{k_2} \\
\Rightarrow E_a = E_b = E_1 = E_2.
\end{aligned} \tag{68}$$

Furthermore, in the massless case for a four vector $\mathbf{p} = (E, \vec{p})$ applies because of the relativistic energy momenta relation:

$$\begin{aligned}
\mathbf{p}^\mu \mathbf{p}_\mu = E^2 - \vec{p} \cdot \vec{p} = m^2 = 0 \\
\Rightarrow E^2 = |p|^2.
\end{aligned} \tag{69}$$

Now it is needed to change the system and get into the "big one" now called "big center of mass" (BCMS) where the protons live, which actually collide. In this system, the whole energy is E_{BCMS} which is the energy that can be set in the experiment as $\sqrt{S}$. To translate between this two systems one can make use of the known energy fraction

x (Bjorken variable) of each parton from the energy of the proton, which leads to the following:

$$E_a + E_b = x_1 E_p + x_2 E_p = (x_1 + x_2) E_p. \tag{70}$$

The proton energy lives in the BCMS and is $E_p = \frac{1}{2} E_{BCMS} = \frac{1}{2}\sqrt{S}$. All the measured variables are measured in the lab system BCMS.

Now the matrix elements are calculated but to get the cross-section there it is useful to take a closer look at the kinematics. Considering equation 3 the cross section is given as:

$$d\sigma = \frac{1}{F} \, |M|^2 \, dPS_n. \tag{71}$$

The matrix elements M were calculated at a parton level (SCMS). But from the experimental perspective there the two protons are colliding (BCMS) and it is not known which parts of the protons are colliding. To solve this problem one needs to consider the parton distributions functions (see ch: 3.6) which gives the following equation[9]:

$$\sigma(AB \to FX) = \sum_{a,b} \int dx_1 \int dx_2 \; P_{a/A}(x_1, Q^2) \; P_{b/B}(x_2, Q^2) \; \hat{\sigma}(ab \to F). \tag{72}$$

So one looks at a collision from a proton A with another proton B, then only collisions which lead to a certain output F, here direct photons, and a rest product X, are taken into consideration. Accordingly, at the parton level all possible collisions (combinations of a and b, which can be quarks and gluons) have to be taken into account and then summed up:

$$\begin{aligned}
\sigma(AB \to FX) = & \int dx_1 \int dx_2 \, P_{Quark/A}(x_1, Q^2) \, P_{Gluon/B}(x_2, Q^2) \, \hat{\sigma}(M_1) \\
& + \int dx_1 \int dx_2 \, P_{Gluon/A}(x_1, Q^2) \, P_{Quark/B}(x_2, Q^2) \, \hat{\sigma}(M_1) \\
& + \int dx_1 \int dx_2 \, P_{Antiquark/A}(x_1, Q^2) \, P_{Gluon/B}(x_2, Q^2) \, \hat{\sigma}(M_2 = M_1) \\
& + \int dx_1 \int dx_2 \, P_{Gluon/A}(x_1, Q^2) \, P_{Antiquark/B}(x_2, Q^2) \, \hat{\sigma}(M_2 = M_1) \\
& + \int dx_1 \int dx_2 \, P_{Quark/A}(x_1, Q^2) \, P_{Antiquark/B}(x_2, Q^2) \, \hat{\sigma}(M_3) \\
& + \int dx_1 \int dx_2 \, P_{Antiquark/A}(x_1, Q^2) \, P_{Quark/B}(x_2, Q^2) \, \hat{\sigma}(M_3).
\end{aligned} \tag{73}$$

Thus, the first two addends correspond to the quark-gluon scattering (4.1.1) the second two to the antiquark-gluon scattering (4.1.2) and the last two to the quark-antiquark scattering (4.1.3). Since we also need to sum over all quarks and antiquarks the formula extends.
Hence, to get the cross section for the protons, $d\sigma$ eq: 71 has to be put in eq: 72:

$$d\sigma(AB \to FX) = \sum_{a,b} \int dx_1 \int dx_2 \, P_{a/A}(x_1, Q^2) \, P_{b/B}(x_2, Q^2) \, \frac{1}{F} \, |M|^2 \, dPS_n. \tag{74}$$

First the integrals need to be transformed. It can be used that the integral above the phase space dPS_n can be written as (see [16]):

$$dPS_n = \frac{1}{(2\pi)^2}\, \delta^4(\mathbf{p} - \mathbf{k_1} - \mathbf{k_2})\, \frac{d^3k_1}{2E_1}\, \frac{d^3k_2}{2E_2}. \tag{75}$$

Here, the momentum p is $\mathbf{p} = \mathbf{p_a} + \mathbf{p_b}$. The idea is to write the whole cross section only depending on the variables k_t (the transversal momentum component of the photon, so of k_2, but from now on just written as k_t), ϕ (the spherical coordinate to k_t, see fig: 13) and the rapidity y_2 also of the photon. These variables are chosen because they are measurable and the depending variables in the experimental data. First the δ distri-

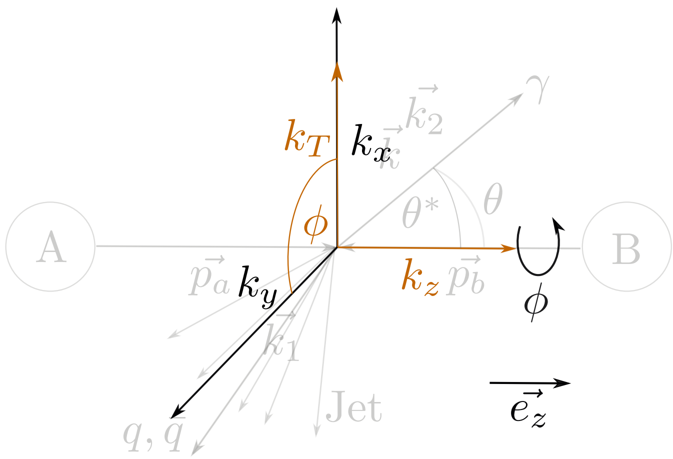

Figure 13: Illustration of the introduction of new spherical coordinates k_T and ϕ.

bution is considered, which basically contains the energy and momentum conservation. The four-dimensional δ-distribution can be splitted into the following four:

$$\begin{aligned}
\delta^4(\mathbf{p} - \mathbf{k_1} - \mathbf{k_2}) =& \delta((x_1 + x_2)E_p - E_1 - E_2) && (76)\\
& \cdot \delta(-k_{1x} - k_{2x}) && (77)\\
& \cdot \delta(-k_{1y} - k_{2y}) && (78)\\
& \cdot \delta((x_1 - x_2)E_p - k_{1z} - k_{2z}). && (79)
\end{aligned}$$

Here is used eq: 70 and that $E_p \approx |p|$ due to the fact that masses are approximated to zero and therefore applying eq: 69. Also $\mathbf{p}$ has no x- nor y-component because the coordinate system is chosen such that $\mathbf{p_a}$ and $\mathbf{p_a}$ and therefore $\mathbf{p}$ only have a z component (see fig: 12). Now every δ distribution is considered separately. Starting with the last (eq: 79):

$$\delta((x_1 - x_2)E_p - k_{1z} - k_{2z}) = \frac{1}{E_p}\, \delta\left(x_1 - x_2 - \frac{k_{1z} + k_{2z}}{E_p}\right) \tag{80}$$

$$\Rightarrow x_1 = x_2 + \frac{k_{1z} + k_{2z}}{E_p}. \tag{81}$$

Now substituting x_1 in equation (76) one gets terms for x_1 and x_2:

$$\begin{aligned}
&\delta\left(\left(2x_2 + \frac{k_{1z}+k_{2z}}{E_p}\right)E_p - E_1 - E_2\right)\\
&= \frac{1}{2E_p}\delta\left(x_2 + \frac{k_{1z}+k_{2z}}{2E_p} - \frac{E_1+E_2}{2E_p}\right) \qquad (82)\\
&\Rightarrow x_2 = \frac{E_1+E_2}{2E_p} - \frac{k_{1z}+k_{2z}}{2E_p} \qquad (83)\\
&\Rightarrow x_1 = \frac{E_1+E_2}{2E_p} + \frac{k_{1z}+k_{2z}}{2E_p}. \qquad (84)
\end{aligned}$$

Then, introducing the rapidity which can be written for a particle of momentum $\mathbf{p_{1,2}}$ as (see [9]):

$$y_{1,2} = \ln\left(\left(\frac{E_{1,2}+k_{1,2z}}{E_{1,2}-k_{1,2z}}\right)^2\right). \qquad (85)$$

x_1 and x_2 can be written as (see A.2.2):

$$\begin{aligned}
x_1 &= \frac{k_T}{2E_p}\left(e^{y_1}+e^{y_2}\right) \qquad (86)\\
x_2 &= \frac{k_T}{2E_p}\left(e^{-y_1}+e^{-y_2}\right). \qquad (87)
\end{aligned}$$

Looking at the cross section (eq: 71) and just analysing the integrals using the δ-distributions to solve the integrals over x_1, x_2, dk_{1x} and dk_{1y} and using $dk_{1z} = E_1\ dy_1$ and $dk_{2z} = E_2\ dy_2$ (app: A.2.4) and introducing spherical coordinates $dk_{2x}dk_{2y} = k_T dk_T d\phi$ (see fig: 13) it follows:

$$\begin{aligned}
&\int dx_1 \int dx_2\ \delta^4(\mathbf{p}-\mathbf{k_1}-\mathbf{k_2})\ \frac{d^3k_1}{2E_1}\ \frac{d^3k_2}{2E_2}\\
&= \frac{1}{4}\frac{1}{2E_p^2}\frac{1}{E_1E_2}\ dk_{2x}\ dk_{2y}\ dk_{2z}\ dk_{1z}\\
&= \frac{1}{2\cdot 4\ E_p^2}\ k_T\ dk_T\ d\phi\ dy_1\ dy_2\\
&= \frac{\pi}{4E_p^2}k_T\ dk_T\ dy_1\ dy_2. \qquad (88)
\end{aligned}$$

Looking at the whole cross section (eq: 71) the pdf's now depend on the rapidities y_1, y_2: $P_{a/A}(x_1, Q^2) = P_{a/A}(y_1, y_2, Q^2)$ used eq: 86 and the same for $P_{b/B}(x_2, Q^2) = P_{b/B}(y_1, y_2, Q^2)$ with eq: 87.

To get the limits for the y_1 integration consider that $x_{1,2} \in [0, 1]$. Zero is only possible if y_1 and y_2 diverge towards minus infinity. Here y_2 is not set to minus infinity (in the experimental comparison y_2 is set close to zero) so $x_{1,2}$ automaticly doesn't become zero. Setting $x_{1,2} = 1$ in eq: 86,87 then one gets the lower and upper limit of y_1 depending on k_T and y_2:

$$\begin{aligned}
y_1 &\le \log\left(\frac{2E_p}{k_T} - e^{y_2}\right) =: y_u\\
y_1 &\ge -\log\left(\frac{2E_p}{k_T} - e^{-y_2}\right) =: y_o. \qquad (89)
\end{aligned}$$

Now the matrix elements M have to be transformed to also only depend on y_1, y_2, k_T. M depends on the mandelstamm variables s, t, u which are considered now in SCMS, so starting with s using that $E_p \approx |\vec{p}|$ (eq: 69):

$$\begin{aligned} s &= (\mathbf{p_a} + \mathbf{p_b})^2 \\ &= ((x_1 + x_2)E_p, (x_1 - x_2)\vec{p})^2 \\ &= \left((x_1 + x_2)^2 - (x_1 - x_2)^2\right) E_p^2 \\ &= 4x_1 x_2 E_p^2. \end{aligned} \tag{90}$$

In SCMS $E_a = E_b$ and $E_1 = E_2$ (eq: 68) and therefore applies:

$$\begin{aligned} s &= (E_a + E_b)^2 = (E_1 + E_2)^2 \\ &= 4E_a^2 = 4E_2^2 \\ &\Rightarrow E_a = E_2 = \sqrt{x_1 x_2} E_p. \end{aligned} \tag{91}$$

Using that θ^{SCMS} is the angle between $\vec{p_a}$ and $\vec{k_2}$ in the SCMS see fig: 14 and as given

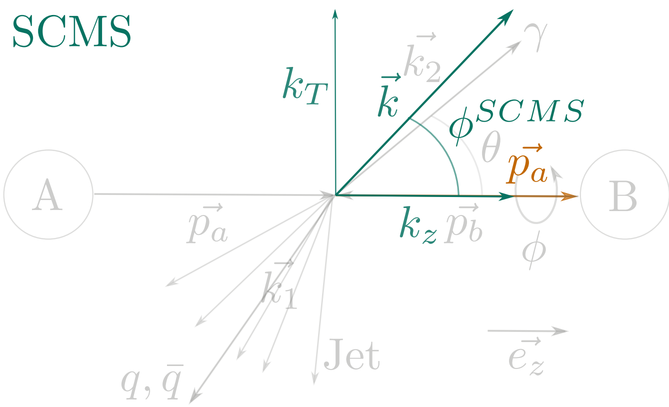

Figure 14: Here the scattering angle ϕ^{SCMS} is illustrated.

in the appendix A.2.3 $\cos(\theta^{SCMS}) = \tanh\left(\frac{y_1 - y_2}{2}\right)$ for u follows:

$$u = -2\ \mathbf{p_a} \cdot \mathbf{k_2}$$

$$= -2E_a\ E_2(1 - \cos(\theta^{SCMS})) \tag{92}$$

$$\begin{aligned} &= -2x_1 x_2\ E_p^2(1 - \cos(\theta^{SCMS})) \\ &= -2x_1 x_2\ E_p^2 \left(1 - \tanh\left(\frac{y_1 - y_2}{2}\right)\right). \end{aligned} \tag{93}$$

t has a sign switch because $\angle(\vec{p_b} \cdot \vec{k_2}) = \pi - \angle(\vec{p_a} \cdot \vec{k_2})$ and becomes:

$$\begin{aligned} t &= -2\ \mathbf{p_b} \cdot \mathbf{k_2} \\ &= -2x_1 x_2\ E_p^2(1 + \cos(\theta^{SCMS})) \\ &= -2x_1 x_2 E_p^2 \left(1 + \tanh\left(\frac{y_1 - y_2}{2}\right)\right). \end{aligned} \tag{94}$$

Finally, the cross sections looks as follows, using that the Flux-factor $F = 4\sqrt{(p_1 \cdot p_2)^2 - m_a^2 m_b^2} = 4E_p^2 \cdot x_1 \cdot x_2$[16] for massless particles and putting eq: 88 in eq: 74:

$$\frac{d\sigma}{dk_T\ dy_2} = \frac{1}{64 \cdot E_p^4\ \pi} \int_{y_u}^{y_o} \sum_{a,b} \frac{P_{a/A}(y_1, y_2, Q^2)}{x_1(y_1, y_2)} \frac{P_{b/B}(y_1, y_2, Q^2)}{x_2(y_1, y_2)} |M_{ab}(y_1, y_2, k_T)|^2 \cdot k_T dy_1 \tag{95}$$

where the matrix element $|M_{a,b}|^2$ has the following form (tab: 2):

a,b	$\lvert M_{a,b}\rvert^2$
quark, gluon	$\lvert M_1\rvert^2 = -\frac{1}{N}(e\ e_f\ g_s)^2 \left(\frac{u}{s} + \frac{s}{u}\right)$
gluon, quark	$\lvert M_1\rvert^2$
antiquark, gluon	$\lvert M_2\rvert^2 = \lvert M_1\rvert^2 = -\frac{1}{N}(e\ e_f\ g_s)^2 \left(\frac{u}{s} + \frac{s}{u}\right)$
antiquark, gluon	$\lvert M_1\rvert^2$
quark, antiquark	$\lvert M_3\rvert^2 = \frac{N^2-1}{N^2}(e\ e_f\ g_s)^2 \left(\frac{t}{u} + \frac{u}{t}\right)$
antiquark, quark	$\lvert M_3\rvert^2$

Table 2: This is an overview of matrix elements $|M_{a,b}|^2$ using the matrix elements from ch: 4.1.

Now only the pdf's have to be put in and the integral to y_1 has to be solved. These computations are done using the programming language python. The sum is over all three processes (M_1, M_2 and M_3) and over all quarks (up, down, charm, strange and bottom).

5. Comparison to data

After the theoretical prediction was evaluated in the last chapter, in this chapter the prediciton is compared to experimental data.

5.1. Experimental background

We start with looking at the experimental background: The prediction is put alongside experimental data from the dissertation "Probing the initial state of heavy-ion collisions with isolated prompt photons" from Florian Jonas (2023)[13]. His results come from the ALICE (A Large Ion Collider Experiment) experiment at the LHC (Large Hadron Collider) at the Cern. The LHC is a synchrotron where particles can be accelerated in two rings and the beams can be collided in four interaction points, one of them is the ALICE experiment. In fig: 15 the schematic construction of the LHC is illustrated, one sees ALICE in one of the four interaction points of the two beams. Dipole magnets accelerate the particles with fields above 8 T. At the LHC particles with the same electric charge can be accelerated which is needed to collide two protons. The ALICE experiment studies QCD and QGP (Quark Gluon Plasma) and is able to identify particles and measures a wide range of transversal momenta. Both is done by 19 subsystems (see fig: 16), which are not discussed further here. To measure direct photons electromagnetic

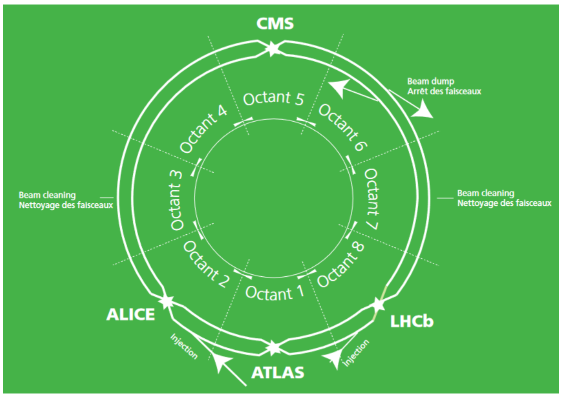

Figure 15: Here one can see a schematic overview of the LHC with the different experiments LHCb, ATLAS, CMS and ALICE [17].

calorimeters (marked in fig: 16) are needed due to the fact that photons undergo electromagnetic interaction. However for the experimental data protons are collided in the

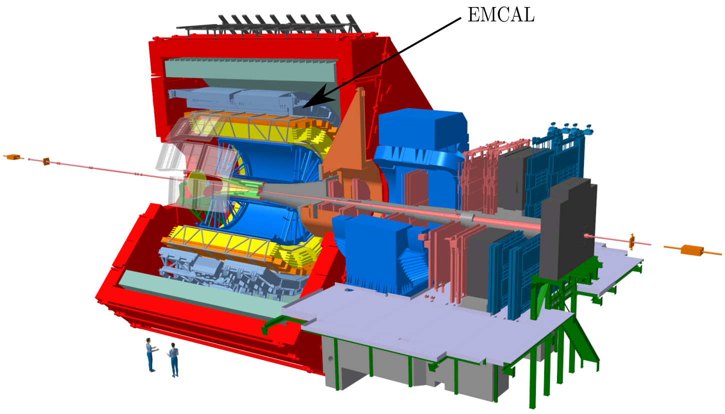

Figure 16: This figure shows the schematic structure of the ALICE experiment[2] with the marked EMCAL i.e. electromagnetic calorimeter.

ALICE experiment which have the energy $\sqrt{S}$=8 TeV (see fig: 17b) which corresponds to the energy of both protons, one proton then has the energy $E_p = \frac{\sqrt{S}}{2}$. The experiment measured a Luminosity $L_{int} = 530.1\,\frac{1}{\text{nb}}$ to get from counted events to the cross section (see eq: 2).

5.2. Numerics

Now the theoretical prediction is to be verified, in this case, better said compared to real data to discuss limitations and strength of the results.
First the prediction has to be completed with the numerics. Therfore, eq: 95 is realized in Python.
Defining parameters: The equation (eq: 95) is full of variables which need to be

defined, starting with the electric charges $e_f e$ and the strong coupling constant g_s[19]:

$$\begin{aligned}\alpha_e &= \frac{1}{137.035999084} \\ e &= \sqrt{4\pi\alpha_e} \qquad (96) \\ \alpha_s(\mu^2) &= 0.1179 \\ g_s &= \sqrt{4\pi\alpha_s}. \qquad (97)\end{aligned}$$

First the strong coupling constant g_s was calculated with eq: 24 which is a first order approximation. To get better results in the final calculations, α_s was taken from the pdf set which has a second order calculation and is used in eq: 97 to get the strong coupling constant. In the sum over a and b (eq: 95) the partons are filled in which are gluon and the quarks up, down, strange, charm, bottom and there antiquarks. Top quark contributions are not relevant for the process since they are highly suppressed due to its high mass (see tab: 1). The electric charges of the quarks e_f are like following (tab: 3):

quark	e_f
up, charm	$\frac{2}{3}$
antiup, anticharm	$-\frac{2}{3}$
down, strange, bottom	$-\frac{1}{3}$
antidown, antistrange, antibottom	$\frac{1}{3}$

Table 3: The table shows the electric charges of the quarks.

The proton energy is set to:

$$E_p = \frac{\sqrt{S}}{2} = 4\,\mathrm{TeV} \qquad (98)$$

like discussed before. In order to compare to the experimental data transversal momenta k_T are chosen between 10 GeV and 80 GeV. The integer N is $N = 3$ for the SU(3) group. And the parameter Q is set to $Q = k_T$, because it has the unit of momenta and k_T relates to the parton system and for practical reasons because then it does not have to be integrated. Q is further discussed in ch: 5.6.1.

Pdf data: The first numerical task is to get the pdf data. The pdf set CT18NNLO[11] and the package LHAPDF[1] is used.

Integration: Secondly, the integration is done by the python routine quad from scipy.integrate. The integral is done for y_1 (rapdity of the jet) in the limits calculated in eq: 89 which depend on y_2 which is set to $y_2 = 0$ so it is in the middle of the given interval between -0.7 and 0.7. Hence, the result is a double differential cross section $\frac{d^2\sigma}{dk_T dy_2}$. To prove that the rapidity y_2 is constant in the observed interval also a second integration over y_2 is done in the limits of the interval between -0.7 and 0.7, then the result is a single differential cross section $\frac{d\sigma}{dk_T}$. The chosen rapidity interval for y_2 (rapidity of the photon) close to zero corresponds to photons scattered along the transversal axis (see $\vec{k_T}$ in fig: 14). The final results are the double differential cross section, bouth double and single are compared in ch: 5.4.

Units: The calculation was done in natural units, meaning $\hbar, c = 1$. To compare to experimental data the result has to be transformed to SI-units. Therefore one introduces a one $(\hbar c)^2 = 0.389\,379\,372\,1\,\mathrm{GeV}^2\mathrm{mb}$[19]. Because the result is wanted in nb the theoretical result $\partial\sigma_{theo}$ has to be multiplied by $0.3894\,10^6\mathrm{GeV}^2$ nb. The units match because the theoretical differential cross section resulted in $\frac{1}{[\mathrm{GeV}^3]}$ multiplying with $[\mathrm{GeV}^2] \cdot \mathrm{c}$ (putting another 1=c on both sides, the momenta then are given in $\frac{\mathrm{GeV}}{\mathrm{c}}$) the result is in the unit $\frac{\mathrm{nb\ c}}{\mathrm{GeV}}$.
In tab: 4 an overview of the corresponding variables of theory and experiment is given.

description	prediction	experimental data
double differential cross section	$\frac{d^2\sigma}{dk_T dy_2}$	$\frac{d^2\sigma}{dp_T dy}$
rapidity of the photon	y_2	y
transverse momentum of the photon	k_T	p_T

Table 4: The table compares the variable names of theoretical prediction and experimental data.

5.3. Comparison of the theoretical prediction and experimental data

Now to discuss the quality of the theoretical prediction, it is compared to real data. Because the quantitative data is not published yet the comparison is only made in a qualitative way, a plot from Florian Jonas' dissertion is used. In fig: 17a the prediction is plotted and on the right (fig: 17b) the experimental data. In both plots the upper plot shows the differential cross section (y-axis) for different momenta on the x-axis. The experimental data is a double differential cross section $\frac{d^2\sigma}{dk_T\ dy}$. The lower plot shows the relative differential cross section. This means the differential cross section is normalized to one and the deviations are shown. The data still depends on the transverse momentum p_T and apparently also on the rapidity of the photon y. How exactly the rapidity dependence was processed is not clear from the work, instead only an interval ($|y| < 0.7$) is indicated. The theoretical prediction is therefore a double differential cross section $\frac{d^2\sigma}{dk_T dy_2}$ with the rapidity set to zero, i.e. $y_2 = 0$. Both results are now given in $\frac{\mathrm{nb\ c}}{\mathrm{GeV}}$. In both the data points are shown with their uncertainties further discussed in section 5.6.

The first thing to note is that the shape of the curves matches qualitatively. The cross section drops sharply with increasing momentum of the photon k_T or p_T. That means that less photons with high kinetic energy are produced, which has different reasons. One is that looking at the pdf's (3.6) for lower transversal momenta k_T which corresponds to lower Bjorken scale x there is a diverging gluon density. Thus, a lot of possible scattering partners decrease fast for higher x. Secondly, because of the chosen interval for the rapidity y_2 the transversal momenta k_T is an energy proxy and therefore to the Bjorken scale x too. Then for small transversal momentum going to zero in the limit the cross section is diverging because of the antiproportional relation of the cross section to x_1 and x_2 (see eq: 95).
To compare the values is difficult because the data is only available in form of a plot, but one can say that the prediction values and data values are in the same order of

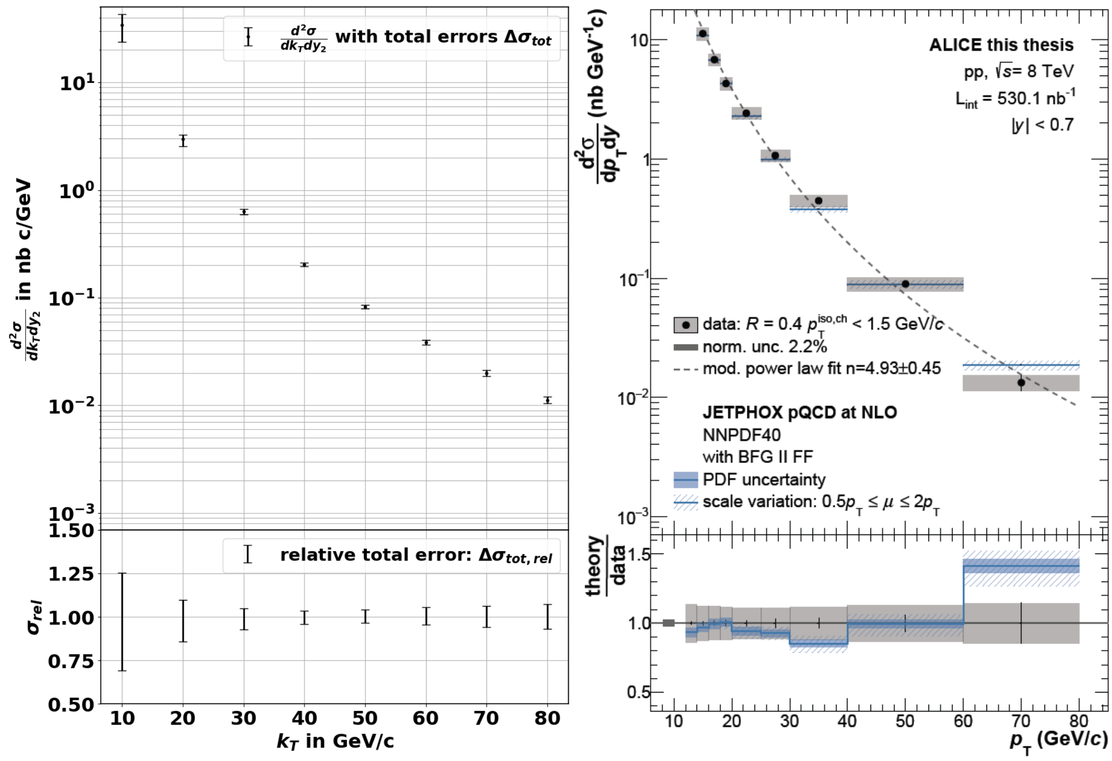

a) Theoretical prediction of the double differential cross section $\frac{d^2\sigma}{dk_T dy_2}$ for $\sqrt{S}$= 8 TeV with the total errors. Below: relative cross section σ_{rel} and relative errors.

b) Experimental data[13] of the cross section $\frac{d^2\sigma}{dp_T dy}$ for $\sqrt{S}$= 8 TeV. Below: relative cross section σ_{rel} and relative errors.

Figure 17: The figure shows the comparison ot the theoretical prediction and experimental data.

magnitude. The theoretical prediction is above the actual measured data points. This might has different reasons which are discussed in the following.

5.4. Prediction limitations

Considering the limitations of the theoretical approach, this deviation is quite satisfactory. First it is unknown how exactly the experimental data were extracted. For the transversal momenta k_T sharp values were taken in the prediction here as well could be an error because the experimental data had to have measured events in a bin of momenta and not at a sharp value of k_T. Thus integrating the momenta bins could improve the results. But a good sign is that the deviation from the experimental data does not increase with increasing k_t corresponding to the increasing bins in the experimental data. In addition it is unclear how the **rapidity dependency** is measured in the experiment. In the theoretical prediction therefore a double differential cross section evaluated at $y_2 = 0$ (the middle of the interval) shown in the comparison above (fig: 17a) and then to check whether the photon rapidity y_2 influences the result, also a single differential cross section is calculated by integrating over y_2 in the given interval, which leads to the following results in fig: 18 compared to the one of the double differential cross section. Like expected the double integrated results are higher on the y-axis. Both could be the base of the experimental data plot, but one does not know.

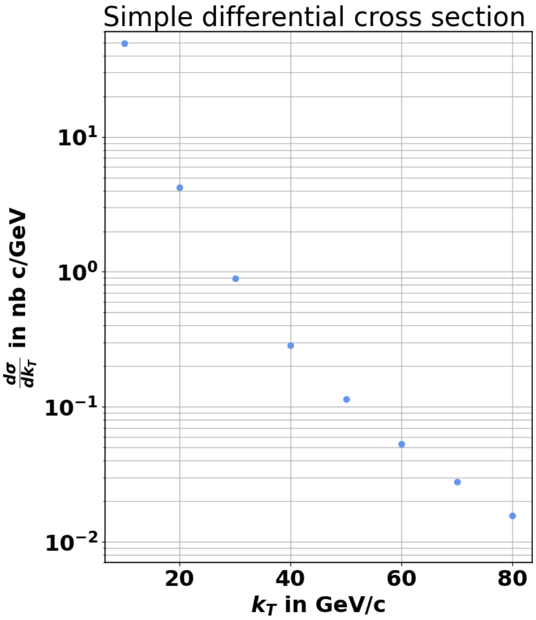

a) The simple differential cross section $\frac{d\sigma}{dk_T}$ is shown.

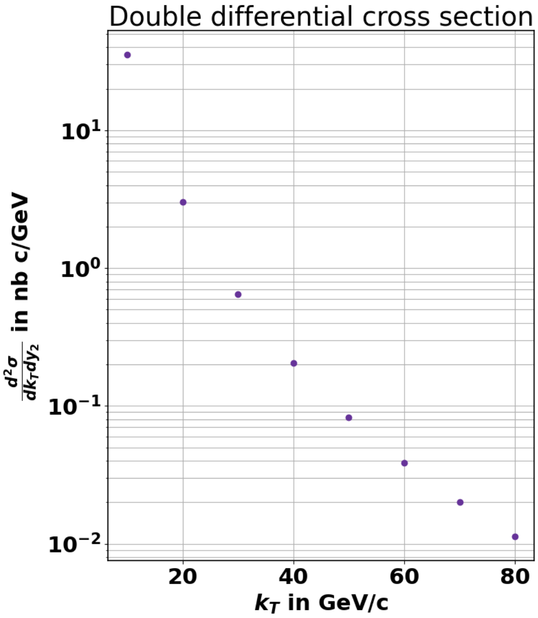

b) The double differential cross section $\frac{d\sigma}{dk_T dy_2}$ is shown.

Figure 18: This figure shows the comparison of the double and simple differential cross section.

To really compare them to the double differential cross section the results have to be divided by the width of the bin $dy = 2 \cdot 0.7 = 1.4$ (fig: 19a). Then both are compared in fig: 19 and it results that both look the same. Checking the numbers of the results shows a small difference (the relative deviation is for each k_T smaller than 1%), which is really small in comparison to the accuracy of the calculation and not even notable in the plot. The relative deviation is shown in fig: 20. The small deviation increases for higher k_T. Thus, maybe y_2 is less constant for higher k_T or it just has to do with the measurement of y_2 one does not know about.
Because of the small difference this comparison shows that the cross section is almost constant in the rapidity bin. From now on the double differential cross section is used for the discussion, because the results of the experiment are given as double differential however it is not known how the rapidity y_2 was dealt with. The used double differential cross section from now on is only called cross section.

A second limit consists in the fact that the experiment is **counting less direct photons** than there actually are. This happens because the experimental set up tries to exclude not-direct photons. One possible way they can be produced is via decay where a pair of photons is produced. To exclude these nondirect photons the experiment only counts photons where there is not a second photon in a certain cone around the first one. (Because of the high velocity of the decaying particle the two photons would be in an close cone.) The experiment though does not count photons which have a second photon in a cone of an certain radius $R = 0.4$ (look fig: 17b). This approach correctly eliminates a lot of not direct photons but also has uncertainty because it also eliminates direct photons which are scattered close to one another coincidentally. To improve the prediction these photons should be cut out of the prediction as well, but require a

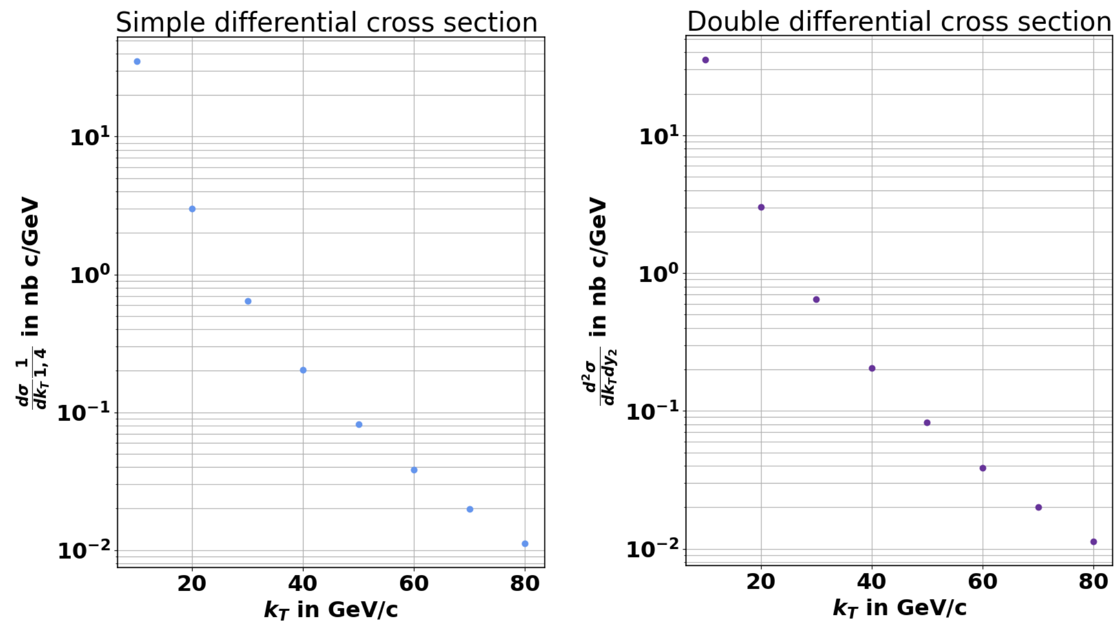

a) The simple differential cross section $\frac{d\sigma}{dk_T}\frac{1}{1.4}$ is shown.

b) The double differential cross section $\frac{d^2\sigma}{dk_T dy_2}$ is shown.

Figure 19: The figure shows the comparison of the double and simple differential cross section including the bin division.

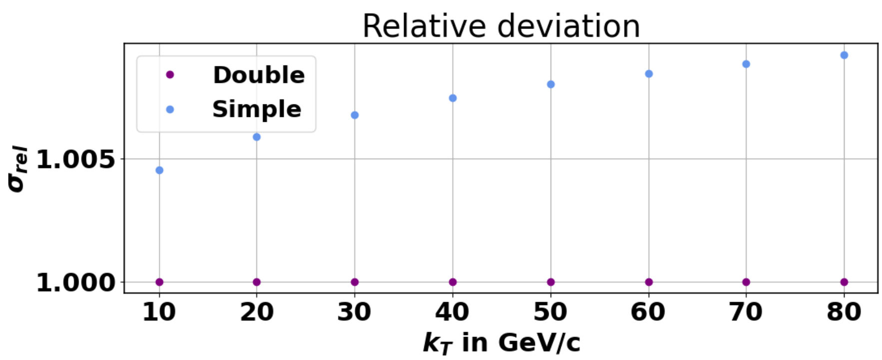

Figure 20: Here the relative cross section for the single and the double differential (the double is set to one) cross section with bin division is shown to illustrate the relative deviation.

deeper dive into quantum chromo dynamics, which exceeds the scope of this work. This improvement would lower the results of the theoretical prediction, which brings them closer to the experimental data.

Another limit is that the calculation of the prediction only includes the **first order**. The feynman diagrams again illustrate this. Only the feynman diagrams fig: 9, 10 and 11 were included. But also diagrams with loops like fig: 8 are possible. To do a first order calculation perturbation theory was used. But to get closer to reality higher orders need to be included in the calculation.
Not only for the matrix elements higher orders are needed but as well for the strong

interaction constant α_s. Eq: 24 is only the first order to get more precision higher orders also need to be included. Thus, first the numerical calculation used eq: 24 with the scale of the Z-boson. To minimize the scale error (ch: 5.6.1) for the final results the coupling constant α_s from the pdf-packages is used, which calculates the α_s including second order.

An additional constraint is that for heavy quarks the **approximation of mass to zero** looses its validity for quarks with higher mass (quark masses in tab: 1). For the up, down and strange quark the mass is in the area of MeV and therefore not relevant but for the charm quark with mass $m_c \approx 1.27$ GeV one cannot safely approximate it to be zero. For the bottom quark $m_b \approx 4.18$ GeV it is the same. Like one sees later especially the charm quark plays a role in the processes so including the masses would improve the prediction.

5.5. Prediction strengths

Like discussed the prediction has some big weaknesses but why is it still useful? First of all, the qualitative shape of the relation can be predicted correct. This is a good indicator that the theoretical prediction about the strong interactions is right.
In addition one can use the model to see the effect each subprocess and each particles has on the overall result and thus the production of direct photons.
First, the three different matrix elements are looked at. Meaning M_1 which corresponds to the quark-gluon scattering, M_2 to the antiquark-gluon scattering and lastly M_3 corresponding to antiquark-quark scattering. In fig: 21 the different relative proportions of the matrix elements in the cross section are plotted. So σ_{rel} is on on the y-axis over the transversal momenta k_T in GeV/c. The shares of the cross section are summed up, so that for example for M_2 at $k_T = 10\,\frac{\text{GeV}}{\text{c}}$ is $\sigma_{rel} \approx 43\%$. The share of the quark-

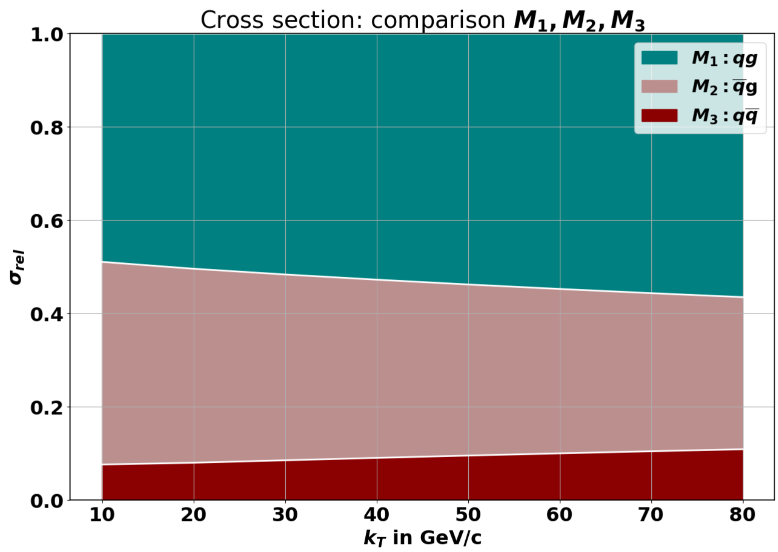

Figure 21: This figure shows the relative cross section for the three processes: Quark-gluon scattering M_1, antiquark-gluon scattering M_2 and quark-antiquark scattering M_3.

gluon scattering is the biggest, which makes sense remembering the pdf's (ch: 3.6), gluons are dominant and quarks are dominant over antiquarks (fig: 6). Then follows antiquark-gluon scattering, here as well gluons are the most probable particle, but antiquarks are less probable than quarks. Lastly, the antiquark-quark scattering has a small share around 0.1 due to the fact that antiquarks are improbable in the proton. Also for small k_T corresponding to little x the gluons get dominant so M_1 and M_2 converge, M_3 goes to zero in the limit. For big k_T and x, M_1 and M_3 increase because the quark gets dominant and the gluons decrease.

Second, the shares of each quark to the cross section for every process M_1, M_2, M_3 are plotted in fig: 22. For M_1 naturally quarks are compared since it is quark-gluon scattering, for M_2 we consider the antiquarks because it is antiquark-gluon scattering, for M_3 then it includes the quark and corresponding antiquark since it is quark-antiquark scattering. The plots confirm the expectation that the up quark is the most frequent

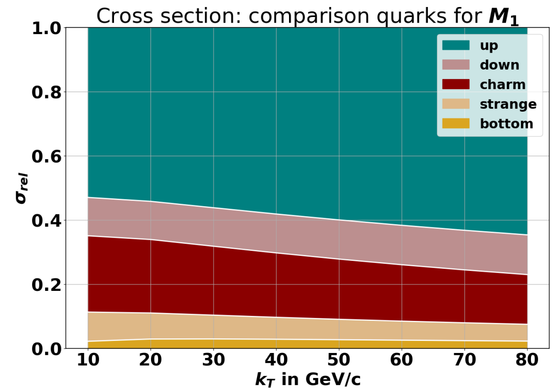

a) This is the relative cross section σ_{rel} for different quarks for M_1.

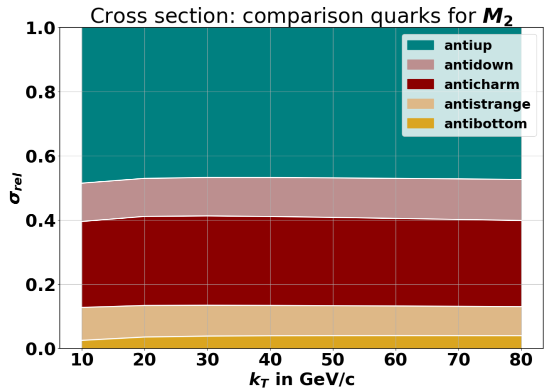

b) This is the relative cross section σ_{rel} for different quarks for M_2.

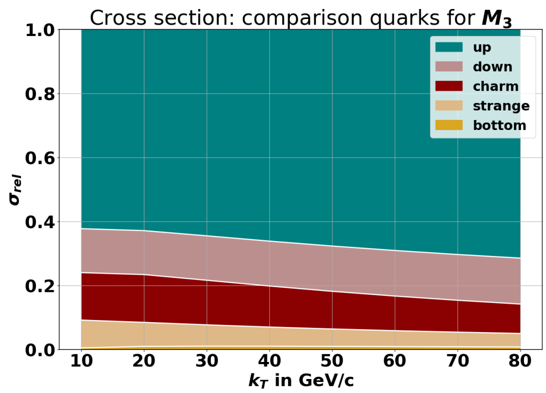

c) This is the relative cross section σ_{rel} for different quarks for M_3.

Figure 22: This figure shows the contributions of the quarks to the cross section for each of the three processes M_1,M_2,M_3.

particle (two up and one down). Hence, one could expect that the second frequent would be the down quark. But one sees that for M_1 and M_2 the charm quark has a higher share than the down quark. This is the case because of the electric charge. Looking at the pdf's (fig: 6) for lower x the share of the charm quark is around half of the down quark (this can be confirmed calculating the cross section with the matrix element $M = 1$). Looking at the electric charges which is $-\frac{1}{3}$ for the down and $+\frac{2}{3}$ for the charm quark squared in the matrix elements (tab: 2) there is a factor 4 in the matrix element, times the factor $\frac{1}{2}$ from the pdf the charm quark's cross section should be around two times larger then the down quark's one which can be seen in the plots (fig: 22a, 22c). Strange and bottom have a low pdf influence and therefore do not contribute much to the cross sections.

Looking at each process for M_1 (fig: 22a) one sees that for higher k_T the influence of the up quarks gets higher which correspond to the pdf's where for higher x the valence quarks get dominant. This is also the reason why the down quarks share increases relatively to the charm quark's one which decreases because of the decreasing pdf for higher x.

For the antiquark-gluon scattering M_2 (fig: 22b) the up quark is dominant then follows charm and then down corresponding to the dominant pdf's (fig: 7) from antidown and antiup quark which cannot be compensated by the electric charge.

Lastly, for the quark-antiquark scattering (fig: 22c) up-quark is dominant again, for low k_T and therefore x charm and down quark have the same share but for higher k_T the relative cross section of the down quark increases due to the raising pdf.

5.6. Uncertainties

The theoretical prediction has two main uncertainties which have been considered: the scale uncercainty and the pdf uncertainty.

5.6.1. Scale-uncertainty

The scale uncertainty exists because as discussed in chapter 3.5 the used Q is only an approximate. It is a free parameter but only if the calculation includes all orders. Thus Q does not has a physical correspond but needs to be chosen to make the calculation by a perturbation theory approach. The parameter Q has units of squared energy or momenta and appears in the nominator in logarithms where the denominator is a function of squared energies and momenta. To choose Q smart then is to approximate this function and to set Q as this approximated value to make the fraction in the logarithm close to one so the logarithm gets close to zero and the Q depends is as small as possible. For higher orders the dependence on Q gets smaller. In consequence for higher orders α_s and the pdf's $P(x, Q)$ (both paremeters depending on Q) get more accurate. Because here only the second order from the coupling constant α_s and pdfs is used the scale of Q gives an uncertainty. The scale uncertainty gets quantified in a certain way which is a convention:

$$\Delta\sigma_Q = \left[\sigma\left(\frac{Q}{2}\right), \sigma(2Q)\right]. \tag{99}$$

In fig: 23a the prediction including the scale uncertainty is shown. It can be seen that the uncertainty decreases with increasing k_T. This is because for higher k_T, which relates to higher impulse fractions x the pdf's decrease and so have less influence on the cross section. The relative error is first decreasing but then increasing again. The scale error has a sign change around 40 GeV implicating that the relative error is decreasing before this point and increasing after it. This sign changes occurs because of the different strength of the Q dependency of the strong coupling constant α_s and the pdf's $P(x, Q)$:

$$M \sim \alpha_s^2\ P(x, Q). \tag{100}$$

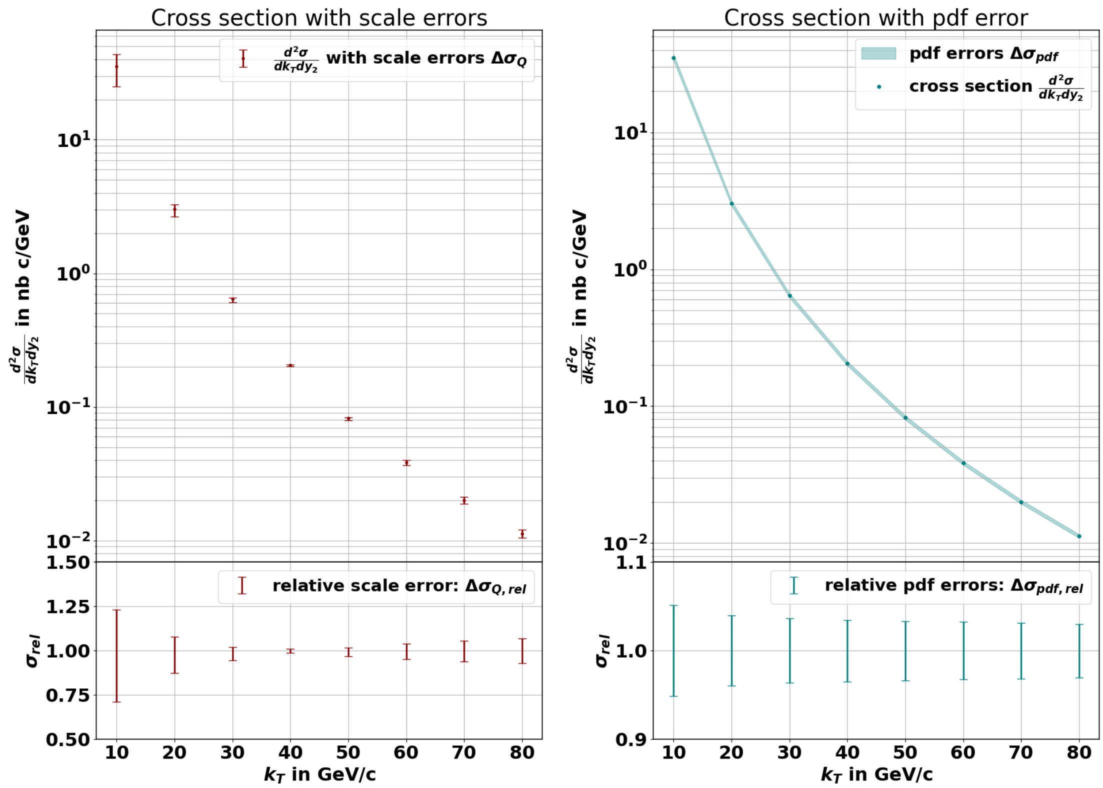

a) Above is shown the cross section $\frac{d^2\sigma}{dk_T dy_2}$ with the scale error and below the relative cross section σ_{rel} and the relative scale error $\Delta\sigma_Q$.

b) Above is shown the cross section $\frac{d^2\sigma}{dk_T dy_2}$ with the pdf error and below the relative cross section σ_{rel} and the relative pdf error $\Delta\sigma_{pdf}$.

Lower Q increase the strong coupling constant α_s and decrease the pdf's $P(x,Q)$. Because of the different strength of the dependency, which is not apparent here now, because both come from the pdf set, there is a sign switch like one sees in the figure 23a.

5.6.2. PDF-uncertainty

The other source of uncertainty are the pdf functions. The pdf's themselves are measured and then fitted values of LHC experiments. Accordingly, they have own uncertainties. The pdf set used here has one central data set and then for 29 fitting parameters an lower and upper value. So to get the uncertainty the difference of the upper value f_k^+ and the lower f_k^- for every parameter k has to be summed up. The uncertainty can be calculated with the following equation[14]:

$$\Delta\sigma_{pdf} = \frac{1}{2}\sqrt{\sum_k (\sigma(f_k^+) - \sigma(f_k^-))^2}. \tag{101}$$

The uncertainties are plotted in figure 23b. The error is lower than the scale error and only about 0.5% to 1.0 % of the cross section σ.

In addition one can look at the cross section for different pdf sets. In the calculation CT18NNLO[11] is used which is a next to next to leading order, meaning two orders calculation, which is now compared to an older version CT14nnlo[6] which is the same just from 2014, also to CT18NLO[11] which is next to leading order so one order and to MSHT20nnlo_mbrange_nf5[4] which is also a next to next to leading order calculation but from different authors and with variation of the bottom quark mass. Fig: 24 shows

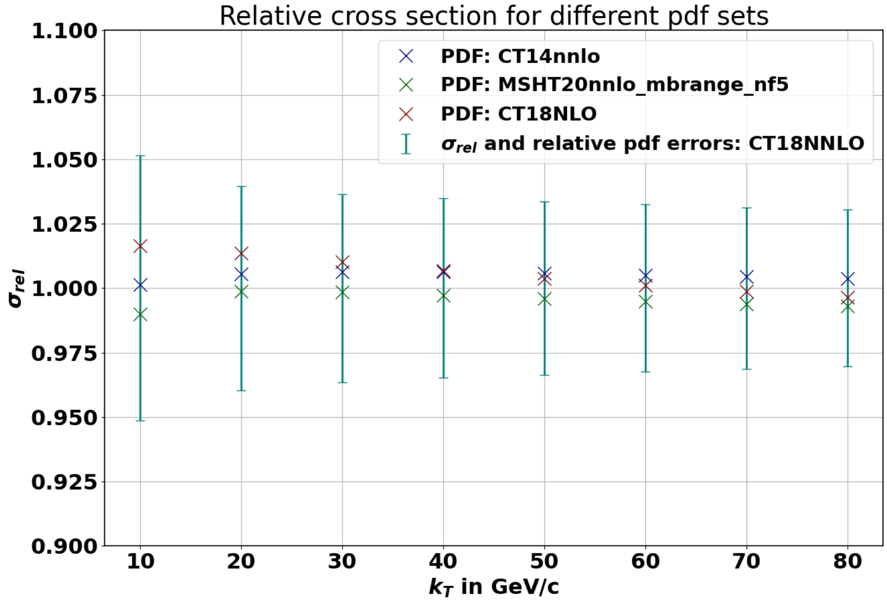

Figure 24: Here the relative cross section σ_{rel} for the used pdf sets with errors and in comparison to three other pdf sets are shown.

that different pdf sets lead to slightly different results for the differential cross section, but within the pdf uncertainty. Hence using different pdf sets influence the results but considering the accurancy of the theoretical prediction it is not crucial.

5.6.3. Total uncertainties

All uncertainties are compared in fig: 25. Scale and pdf error are in the same scale of magnitude. It turns out that first (for lower k_T) the scale error $\Delta\sigma_Q$ is dominant, around k_T=40 GeV the pdf uncertainty $\Delta\sigma_{pdf}$ is dominant but at k_T=60 GeV the scale error $\Delta\sigma_Q$ gets dominant again (see fig: 25). The total error is calulated with the following equation[14]:

$$\Delta\sigma_{tot} = \sqrt{\Delta\sigma_Q^2 + \Delta\sigma_{pdf}^2 + \Delta\sigma_{int}^2}. \tag{102}$$

Theoretically there also is a numerical uncertainty from the integration. But the precision is increased till the integration uncertainty becomes small compared to the other uncertainties and therefore gets irrelevant.

6. Conclusion

Concluding, this thesis could retrace how direct photons are produced in proton-proton collisions at the LHC. The direct photons are a product of the strong interaction of quarks and gluons inside the proton while the quark interacts electromagneticly at the same time and therefore produces a photon.
For the prediction therefore feynman rules of strong and electromagnetic interaction are

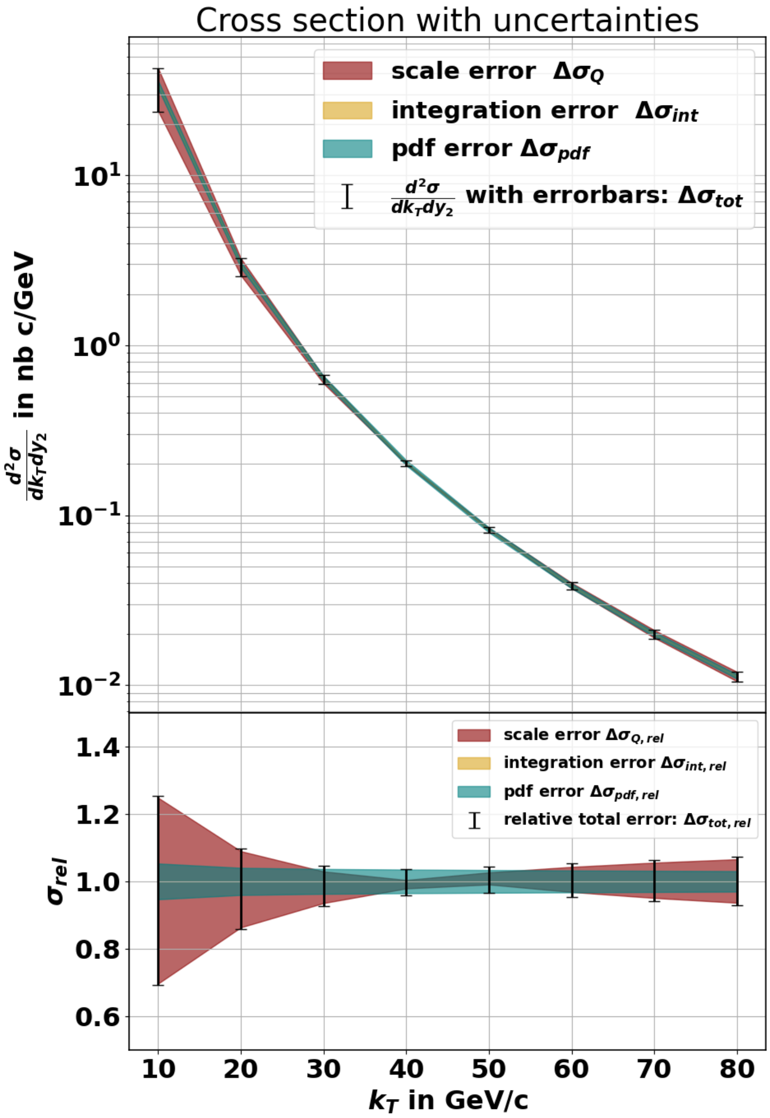

Figure 25: The figure shows the theoretical prediction for the cross section $\frac{d^2\sigma}{dk_T dy_2}$ with all uncertainties, named scale error, pdf error and integration error. Below the relative cross section σ_{rel} with the relative errors is plotted.

used following from the Lagrangian and perturbation theory. There are three processes quark-gluon scattering, antiquark-gluon scattering and antiquark-quark scattering that produce a direct photon and therefore need to be considered. The prediction is then made for $\sqrt{S}$=8 TeV corresponding to the experimental data. The theoretical results match on a qualitatively level successfully the experimental data with an upward shift. The discussion reveals that looking only at first order, setting the masses to zero and including photons not counted from the experiment due to the exclusion cone are limits of the prediction, which are also the possibilities to get better results. Even though this massless first order prediction shows the right shape of the decrease of the cross section for increasing photon momenta. In addition one can predict correctly that the quark-gluon scattering M_1 is the most probable process followed by antiquark-gluon scattering M_2 for lower photon momenta k_T. For higher k_T the trend that the antiquark-quark scattering increases is visible as well. This allows important conclusions to be drawn

about the proton structure: Gluons are more frequent for lower transversal momenta k_T and decrease for higher k_T. Quarks are more frequent than antiquarks and for higher k_T get dominant against gluons. The comparison of the quarks shows that up quarks are the most frequent. The second biggest contribution to the cross section have the charm quarks which is because of their bigger electric charge which compensate their less frequent existence in the pdfs. Considering the electric charges one still can confirm that protons consist of two up quarks and one down quark.
All in all, much could be learned about LHC physics in this thesis. Starting how cross sections are calculated theoretically and broaching quantum chromo dynamics. Especially, how to make a prediction in a way which makes a comparison of experimental data and theoretical results possible could be studied and also which limitations simplified calculations like this one have, could be studied.

A. Appendix

A.1. γ-matrices

The γ-matrices or also called Dirac matrices because they were introduces in the dirac equation and underly the dirac algebra. They have the following identities:

$$\begin{aligned}
\{\gamma^\mu, \gamma^\nu\} &= 2g^{\mu\nu}\mathbf{1} \\
(\gamma^\mu)^\dagger &= \gamma^0\gamma^\mu\gamma^0 \\
(\gamma^\mu)^2 &= \mathbf{1} \\
\gamma^\mu\gamma_\mu &= 4 \\
\gamma^\mu\gamma^\alpha\gamma_\mu &= -2\gamma^\alpha \\
\gamma^\mu\gamma^\alpha\gamma^\beta\gamma_\mu &= 4g^{\alpha\beta} \\
\gamma^\mu\gamma^\alpha\gamma^\beta\gamma^\delta\gamma_\mu &= -2\gamma^\delta\gamma^\beta\gamma^\alpha,
\end{aligned} \tag{103}$$

$$\begin{aligned}
\mathrm{Tr}[\gamma^\mu] &= 0 \\
\mathrm{Tr}[\gamma^\mu\gamma^\nu] &= 4g^{\mu\nu} \\
\mathrm{Tr}[\gamma^\mu\gamma^\nu\gamma^\rho] &= 0 \\
\mathrm{Tr}[\gamma^\mu\gamma^\nu\gamma^\rho\gamma^\sigma] &= 4(g^{\mu\nu}g^{\rho\sigma} - g^{\mu\rho}g^{\nu\sigma} + g^{\nu\rho}g^{\mu\sigma}).
\end{aligned} \tag{104}$$

Relations between u,v and γ-matrices:

$$\begin{aligned}
\bar{u}(p) &= u^+(p)\gamma^0 \\
\bar{\psi}(x) &= \psi^+\gamma^0 \\
\bar{v}(p) &= v^+(p)\gamma^0.
\end{aligned} \tag{105}$$

A.2. Kinematics

A.2.1. Mandelstamm variables

$$\begin{aligned}
s &= (\mathbf{p_1} + \mathbf{p_2})^2 = (\mathbf{k_1} + \mathbf{k_2})^2 \\
t &= (\mathbf{p_1} - \mathbf{k_1})^2 = (\mathbf{p_2} - \mathbf{k_2})^2 \\
u &= (\mathbf{p_1} - \mathbf{k_2})^2 = (\mathbf{p_2} - \mathbf{k_1})^2
\end{aligned} \tag{106}$$

$$\begin{aligned}
s + t + u &= \mathbf{p_1}^2 + \mathbf{p_2}^2 + \mathbf{k_1}^2 + \mathbf{k_2}^2 \\
&= m_1^2 + m_2^2 + m_3^2 + m_4^2
\end{aligned} \tag{107}$$

A.2.2. Subcalculation x_1 and x_2

Starting from:

$$\begin{aligned}
x_2 &= \frac{E_1 + E_2}{2E_p} - \frac{k_{1z} + k_{2z}}{2E_p} \\
x_1 &= \frac{E_1 + E_2}{2E_p} + \frac{k_{1z} + k_{2z}}{2E_p}.
\end{aligned} \tag{108}$$

Looking at the rapdities y_1, y_2 and using the conversion below (eq: 110) and that $k_T^2 = k_x^2 + k_y^2$:

$$e^{\pm y_{1,2}} = \sqrt{\frac{E_{1,2} \pm k_{1,2z}}{E_{1,2} \mp k_{1,2z}}} = \frac{E_{1,2} \pm k_{1,2z}}{k_{1,2T}} \tag{109}$$

$$\begin{aligned} \frac{E_{1,2} \pm k_{1,2z}}{E_{1,2} \mp k_{1,2z}} &= \frac{(E_{1,2} \pm k_{1,2z})^2}{(E_{1,2} \mp k_{1,2z})(E_{1,2} \pm k_{1,2z})} \\ &= \frac{(E_{1,2} \pm k_{1,2z})^2}{E_{1,2}^2 - k_{1,2z}^2} \\ &= \frac{(E_{1,2} \pm k_{1,2z})^2}{k_{1,2x}^2 + k_{1,2y}^2 + k_{1,2z}^2 - k_{1,2z}^2} \\ &= \frac{(E_{1,2} \pm k_{1,2z})^2}{k_{1,2T}^2} \end{aligned} \tag{110}$$

Comparing eq: 109 with eq: 108 x_1 and x_2 can be written as:

$$x_1 = \frac{k_T}{2E_p}\left(e^{y_1} + e^{y_2}\right) \tag{111}$$

$$x_2 = \frac{k_T}{2E_p}\left(e^{-y_1} + e^{-y_2}\right). \tag{112}$$

A.2.3. Scattering angle θ

The following relation is to be proved:

$$\cos(\theta^{SCMS}) = \tanh\left(\frac{y1 - y2}{2}\right). \tag{113}$$

The angle θ^{SCMS} lives in the SCMS. Then a look at the rapidities is needed. The rapidities y_1 (from the jet) and y_2 from the photon live in BSCMS, in the SCMS there is a shift y^*:

$$y_{1,2} = y_{SCMS} \pm y^* \tag{114}$$

$$\Rightarrow y^* = \frac{1}{2}(y_1 - y_2). \tag{115}$$

Hence θ^{SCMS} corresponds to the shift from the SCMS and to $\vec{k_{1,2}^{SCMS}}$. In the following equation $k_{1,2}^{SCMS}$ is written as just k (in SCMS $\vec{k_1}$ and $\vec{k_2}$ are the same apart from an minus sign, which does not matter for the angle), also $|k| \approx E$ and eq: 109 are used in fig: 14 one sees that for θ^{SCMS} applies:

$$
\begin{aligned}
\cos(\theta^{SCMS}) &= \frac{k_z}{|k|} \\
&= \frac{2k_z}{\sqrt{(|k|-k_z)(|k|+k_z)}} \frac{\sqrt{(|k|-k_z)(|k|+k_z)}}{2k_z} \\
&= \left(\sqrt{\frac{|k|+k_z}{|k|-k_z}} - \sqrt{\frac{|k|-k_z}{|k|+k_z}}\right) \left(\sqrt{\frac{|k|+k_z}{|k|-k_z}} + \sqrt{\frac{|k|-k_z}{|k|+k_z}}\right)^{-1} \\
&= \left(e^y - e^{-y}\right) \frac{1}{e^y + e^{-y}} \\
&= \frac{\sinh(y)}{\cosh(y)} = \tanh(y) = \tanh\left(\frac{y_1 - y_2}{2}\right). \qquad (116)
\end{aligned}
$$

Looking at fig: 14 on also sees that:

$$
|k_2| = \frac{k_T}{\sin(\theta^{SCMS})}. \qquad (117)
$$

A.2.4. Subcalculation integral

Transforming the integral over k_z-component to the rapidity using [16].

$$
\begin{aligned}
\frac{dy}{dk_z} &= \left(\frac{\partial y}{\partial k_z} + \frac{\partial y}{\partial E}\frac{\partial E}{\partial k_z}\right) \\
&= \frac{E}{E^2 - k_z^2} - \frac{k_z}{E^2 - k_z^2}\frac{k_z}{E} \\
&= \frac{1}{E} \qquad (118)
\end{aligned}
$$

This applies for k_{1z} and k_{1z} and leads to:

$$
\frac{1}{E_{1,2}} dk_{z1,2} = dy_{1,2}. \qquad (119)
$$

References

[1] Andy Buckley et al. “LHAPDF6: parton density access in the LHC precision era”. In: *The European Physical Journal C* 75 (2015), pp. 1–20.

[2] CERN. URL: `https://alice.cern/experiment` (visited on 08/01/2023).

[3] Wikimedia Commons. URL: `https://de.wikipedia.org/wiki/Datei:Standard_Model_of_Elementary_Particles-de.svg` (visited on 08/14/0023).

[4] T Cridge et al. “An investigation of the α _S α S and heavy quark mass dependence in the MSHT20 global PDF analysis”. In: *The European Physical Journal C* 81 (2021), pp. 1–29.

[5] Alexandre Deur, Stanley J Brodsky, and Guy F de Téramond. “The QCD running coupling”. In: *Progress in Particle and Nuclear Physics* 90 (2016), pp. 1–74.

[6] Sayipjamal Dulat et al. “New parton distribution functions from a global analysis of quantum chromodynamics”. In: *Physical Review D* 93.3 (2016), p. 033006.

[7] R Keith Ellis, W James Stirling, and Bryan R Webber. *QCD and collider physics*. Cambridge university press, 2003.

[8] Francis Halzen and Alan D Martin. *Quark & Leptons: An introductory course in modern particle physics*. John Wiley & Sons, 2008.

[9] Tao Han. “Collider phenomenology: Basic knowledge and techniques”. In: *Physics In D 4 Tasi 2004: TASI 2004*. World Scientific, 2006, pp. 407–454.

[10] Wolfgang Hollik. “Quantum field theory and the Standard Model”. In: *arXiv preprint arXiv:1012.3883* (2010).

[11] Tie-Jiun Hou et al. “Progress in the CTEQ-TEA NNLO global QCD analysis”. In: *arXiv preprint arXiv:1908.11394* (2019).

[12] Wolfram Research, Inc. *Mathematica, Version 13.3*. Champaign, IL, 2023. URL: `https://www.wolfram.com/mathematica`.

[13] Florian Jonas. “Probing the initial state of heavy-ion collisions with isolated prompt photons”. In: *Institut für Kernphysik Westfälische Wilhelms-Universität Münster* (2023).

[14] K Kovařík et al. “nCTEQ15: Global analysis of nuclear parton distributions with uncertainties in the CTEQ framework”. In: *Physical Review D* 93.8 (2016), p. 085037.

[15] Karol Kovařík. “From Quantum Mechanics To Quantum Chromodynamics - The Path Integral Approach”. In: ().

[16] Karol Kovařík. *Hitchhiker’s Guide to Renormalization*. unpublished, 2021.

[17] Ana Lopes and Melissa Loyse Perrey. *FAQ-LHC The guide*. Tech. rep. 2022.

[18] Jakob Schwichtenberg. *Physics from symmetry*. Springer, 2018.

[19] R. L. Workman and Others. “Review of Particle Physics”. In: *PTEP* 2022 (2022), p. 083C01. DOI: `10.1093/ptep/ptac097`.

Declaration of Academic Integrity

I hereby confirm that this thesis, entitled ____

____ is solely my own work and that I have used no sources or aids other than the ones stated. All passages in my thesis for which other sources, including electronic media, have been used, be it direct quotes or content references, have been acknowledged as such and the sources cited. I am aware that plagiarism is considered an act of deception which can result in sanction in accordance with the examination regulations.

____

(date, signature of student)

I consent to having my thesis cross-checked with other texts to identify possible similarities and to having it stored in a database for this purpose.

I confirm that I have not submitted the following thesis in part or whole as an examination paper before.

____

(date, signature of student)